

# Transition Metals in Gale Crater, Mars: Perspectives on Global Abundances and Future Exploration

Valérie Payré<sup>1</sup>, Marion Nachon<sup>2</sup>, Roger C. Wiens<sup>3</sup>, Jérémie Lasue<sup>4</sup>, Mark Salvatore<sup>1</sup>, Ann M. Ollila<sup>5</sup>, Nina L. Lanza<sup>3</sup>, and Pierre-Yves Meslin<sup>4</sup>

<sup>1</sup>Northern Arizona University

<sup>2</sup>Texas A&M University

<sup>3</sup>Los Alamos National Laboratory (DOE)

<sup>4</sup>IRAP-OMP

<sup>5</sup>Los Alamos National Laboratory

November 22, 2022

## Abstract

Through rover missions and martian meteorites received on Earth, the surface of Mars has showed unexpectedly elevated concentrations of transition metals usually measured in minor and trace concentrations in silicate rocks compared to the average crust. Gale crater presents one of the most diverse geological records in terms of its complex fluid and magmatic history described through the sedimentary and igneous records, respectively. Transition metals, such as Mn, Co, Ni, Cu, and Zn, are highly concentrated within various sedimentary rocks and diagenetic features, suggesting their mobilization through fluid circulation. This paper presents the first compilation of elevated concentrations of transition metals measured by the *Curiosity* rover and reviews the origin of such metals in Gale crater, highlighting the existence of a hydrothermal or magmatic-hydrothermal deposit in its vicinity. The discovery of felsic magmatism on Mars opens up to novel perspectives in terms of the type of metal deposits that current and future exploration could evidence at the surface of Mars and raise questions about the global abundance of such metals. Constraining the abundance of transition metals is also a central question for exobiology purposes. Because on Earth living organisms use transition metals for their survival and functioning, should life have arisen on Mars, the availability of such chemical elements at the surface could have been essential for its development. An accurate assessment of *in situ* metal resources and potential risks for health will be key for the preparation of human exploration of Mars as recently announced by NASA.

## Hosted file

metals\_gale\_crater\_tables.docx available at <https://authorea.com/users/534616/articles/598517-transition-metals-in-gale-crater-mars-perspectives-on-global-abundances-and-future-exploration>

# **Transition Metals in Gale Crater, Mars: Perspectives on Global Abundances and Future Exploration**

V. Payre<sup>1</sup>, M. Nachon<sup>2</sup>, R. C. Wiens<sup>3</sup>, J. Lasue<sup>4</sup>, M. Salvatore<sup>1</sup>, A. M. Ollila<sup>3</sup>, N. L. Lanza<sup>3</sup>,  
and P.-Y. Meslin<sup>4</sup>.

<sup>1</sup>Department of Astronomy and Planetary Science, Northern Arizona University, Flagstaff  
AZ ([valerie.payre@nau.edu](mailto:valerie.payre@nau.edu))

<sup>2</sup>Department of Geology and Geophysics, Texas A&M University, College Station TX

<sup>3</sup>Los Alamos National Laboratory, Los Alamos NM

<sup>4</sup>Institut de Recherche en Astrophysique et Planétologie, Université Paul Sabatier,  
Toulouse, France

## **Key Words**

Mars, metals, metal deposit, life, human exploration

## **Key Points** (*140 characters*)

- Results from Gale crater suggest a hydrothermal or magmatic-hydrothermal transition metal deposit located somewhere in its watersheds
- The diversity of magmatic processes from mafic to felsic widens the type of metal deposits expected, possibly as diverse as on Earth
- The abundance of transition metals is crucial to evaluate the development of potential living organisms and the toxicity for human

## Abstract (250 words)

Through rover missions and martian meteorites received on Earth, the surface of Mars has showed unexpectedly elevated concentrations of transition metals usually measured in minor and trace concentrations in silicate rocks compared to the average crust. Gale crater presents one of the most diverse geological records in terms of its complex fluid and magmatic history described through the sedimentary and igneous records, respectively. Transition metals, such as Mn, Co, Ni, Cu, and Zn, are highly concentrated within various sedimentary rocks and diagenetic features, suggesting their mobilization through fluid circulation. This paper presents the first compilation of elevated concentrations of transition metals measured by the *Curiosity* rover and reviews the origin of such metals in Gale crater, highlighting the existence of a hydrothermal or magmatic-hydrothermal deposit in its vicinity. The discovery of felsic magmatism on Mars opens up to novel perspectives in terms of the type of metal deposits that current and future exploration could evidence at the surface of Mars and raise questions about the global abundance of such metals. Constraining the abundance of transition metals is also a central question for exobiology purposes. Because on Earth living organisms use transition metals for their survival and functioning, should life have arisen on Mars, the availability of such chemical elements at the surface could have been essential for its development. An accurate assessment of *in situ* metal resources and potential risks for health will be key for the preparation of human exploration of Mars as recently announced by NASA.

## Plain Language Summary (200 words)

Carbon, hydrogen, nitrogen, oxygen, phosphorus, and sulfur are the foundations of any living organisms. Additional elements including transition metals like Mn, Co, Ni, Cu, and Zn, are required for organisms survival and sustainability, if not playing a key role in the prebiotic synthesis of essential molecules like the ribonucleic acid. At the surface of Mars, rover missions including the *Curiosity* rover demonstrated the existence of a variety of such metals with elevated abundances measured in a variety of rocks. In Gale crater, the circulation of hydrothermal fluids, and surface and ground waters accumulated transition metals within sediments, demonstrating the existence of metal deposits at the surface of Mars that would be beneficial for the development of potential life. The wide diversity of Mars' magmatic processes highlighted these past few years expands the type of metal deposits that could be encountered on Mars in future explorations. From the development of life to future human exploration, the assessment of metal abundance at the surface of Mars is fundamental as metals are vital as well as toxic for living organisms including astronauts, and the Mars 2020 and follow-up sample return missions will be essential regarding the metal distribution at Mars' surface and interior.

## 1. Introduction

By definition, a metal is an element with high thermal and electrical conductivity and corresponds to all elements in the Mendeleiev table except for noble gases and halogens. In this paper, we will focus on transition metals that are typically in minor and trace concentrations (0.1-1 wt. % and < 1000 ppm, respectively) in silicate rocks. The search for abundant metal resources among all attainable planetary bodies is now of interest, especially for technological applications. In addition to being lucrative as natural resources, transition metals are also of significance for scientists when exploring the history of a planet. How did a planetary body form? Was a planetary body once a habitable world? The delicate affinities between transition metal elements provide essential clues into geological processes that are otherwise puzzling to understand using other elements, such as planetary differentiation processes, impacts, and hydrothermal and diagenetic processes. Geological processes that concentrate or deplete certain metals can be deduced from elemental ratios and metal concentrations. Transition metals by themselves are vital for the development of life and its sustainability and estimating the distribution of metals on planetary bodies is imperative in understanding whether extra-terrestrial life could have ever existed in our solar system. The increasing numbers of rover and orbital missions to Mars, and the martian meteorites discovered on Earth, allow us to draw a more precise knowledge of the abundance of metals on Mars.

Studies of martian meteorites mainly use transition metal abundances to explore the differentiation of Mars, including core formation and the contribution of impactors (e.g., Humayun et al., 2013; Yang et al., 2015). Magmatic metal-bearing sulfides commonly exist at low abundances within martian meteorites (e.g., Baumgartner et al., 2017; Lorand et al., 2005). Elevated concentrations of transition metals have been observed in some meteorites including the martian brecciated meteorite Northwest Africa NWA 7533 that displays high Ni (up to 2.8 wt.%) compared to the average martian crust (Table 1) and nuggets of Highly Siderophile Elements (HSE) within hydrothermal pyrite grains, likely supplied by chondritic impactor debris (J. -P. Lorand et al., 2018; Jean-Pierre Lorand et al., 2015). Orbital observations cannot resolve the concentrations of transition metals in trace amounts at the surface of Mars. Chalcophile and siderophile metals that prefer sulfur and iron metal phases, respectively, might exist in association with sulfate and iron-oxide minerals detected by orbital spectroscopic analyses such as the Compact Reconnaissance Imaging Spectrometer for Mars (CRISM) aboard the Mars Reconnaissance Orbiter (MRO). However, no study that we are aware of discusses the occurrence from orbital observations of minerals containing transition metals that are

usually in minor and trace amounts in silicate rocks (e.g., Cr, Mn, Co, Ni, Cu, Zn), like sphalerite or chalcopyrite. In Gusev crater and at Meridiani Planum (Fig.1), the Mars Exploration Rovers (MERs) measured elevated concentrations of Zn (up to 6,200 ppm) associated with Ge, suggesting high-temperature fluid circulation ( $> 150^{\circ}\text{C}$ ) that occurred as either hydrothermalism or volcanic vapor condensation (Ming et al., 2008; Squyres et al., 2007, 2012), while high Ni contents (up to 2,100 ppm) were interpreted as contributions from an impactor (Ming et al., 2008). Such metal concentrations differ dramatically from the average compositions of the martian crust and that of the primitive mantle (Table 1). In Gale crater (Fig.1), the Mars Science Laboratory (MSL) *Curiosity* rover measured the strongest variability of transition metal abundances ever observed on the ground for Zn, Cu, and Ni, highlighting a complex fluid history. All these observations raise a central question regarding metals on Mars: How abundant are transition metals at the surface of Mars and how are they distributed? Such information is fundamental regarding (1) the habitability of the planet, i.e., the capacity of a planet to support the emergence of life (Cockell et al., 2016) as transition metal availability at the surface and subsurface is essential for the development of life, and (2) human exploration, since transition metals are essential for sustainable agriculture and food production. On the other hand, elevated metal concentrations are toxic for humans. Having an estimation of these metal abundances is essential when looking ahead to human martian exploration and possible in situ resource utilization.

This manuscript presents the first compilation of all rocks and soils in Gale crater presenting elevated concentrations of transition metals as measured by instruments onboard the *Curiosity* rover and aims to review and discuss environmental conditions that concentrated these elements in some locations. We will focus on minor and trace transition metals Mn, Cu, Zn, and Ni detected and measured by various instruments onboard the *Curiosity* rover. A projection of the extent of some transition metals at the surface of Mars will be discussed, followed by a review of the importance of metals for living organisms and for human exploration.

## **2. The *Curiosity* Rover in Gale Crater**

Gale crater located on the dichotomy boundary between the southern highlands and the northern lowlands (Fig.1), exposes a uniquely preserved geological diversity reflected by the variety of rocks analyzed by the *Curiosity* rover and the large compositional range of both igneous and sedimentary rocks. With a record number of modern analytical instruments onboard *Curiosity*, an unprecedented array of minor and trace transition metals can be now

detected and quantified, including Cr, Mn, Co, Ni, Cu, and Zn. This section reviews the geological context of the formations presenting abnormally elevated transition metal concentrations, and present the suggested processes that concentrated them in those materials.

Throughout the paper, we define “high” or “elevated” abundances when their value is three times higher than those estimated in the average martian crust (Table 1; Taylor and McLennan, 2009). Table S1 and S2 present the first compilation of all targets available that contain elevated concentrations of transition metals compared to the average crust, as measured by the *Curiosity* rover, and is the support of our geological review. Table 2 and 3 are a simplified version with the highest concentration of transition metals measured in each Gale crater formation.

## 2-1. Elemental and Mineralogical Analyses

Onboard the *Curiosity* rover, the instruments providing elemental and mineralogical analyses are the Chemistry Camera (ChemCam) and the Alpha Particle X-Ray Spectrometer (APXS) to study chemistry, and CheMin, which is an X-ray diffractometer (XRD) designed to provide quantitative mineralogy of drilled and sieved rocks. ChemCam uses laser-induced breakdown spectroscopy (LIBS) to analyze, at distance (up to 7 m away from the rover), the elemental composition of rocks at a sub-millimeter scale (spot size: 350-550  $\mu\text{m}$ ; Maurice et al., 2012; Wiens et al., 2012). For each target analyzed by LIBS, several points of analyses are acquired across the target, typically in raster of 5 to 10 individual points per target. For each individual point of analysis, a total of 30 laser shots are usually acquired on the same point of analysis, removing the dust cover at the surface and ablating a few  $\mu\text{m}$  into the rock or soil (A. Cousin et al., 2011). For the calculation of chemical composition, the first five LIBS emission spectra of each point of analysis are excluded as they are typically dominated by dust contributions, and the remaining spectra are averaged. ChemCam also consists of a high resolution Remote Micro Imager (RMI) to contextualize LIBS measurements. The APXS determines elemental abundances from a derived X-ray spectrum excited by an alpha-particle source, with a footprint of 1.6 cm (Gellert et al., 2015). CheMin obtains its diffraction pattern from samples that are drilled and (usually) sieved by the rover (Blake et al., 2012). At the time of this writing, ChemCam has made more than 30,000 rock and soil observations as individual points in raster of usually 5 to 10 per target; APXS has made about a thousand observations, usually as single measurements with varying integration times; and CheMin has analyzed material from ~30 drill holes and several scoops of soil.

Table S1 is a compilation of transition metal abundances measured by ChemCam collected from various studies to martian day (sol) 2608 (Mn: Gasda et al., 2019; Lanza et al., 2016,

2014; Zn: Lasue et al., 2016; Cu: Payré et al., 2019; Ni: Johnson et al., 2021, 2020; Lasue et al., 2020; Meslin et al., 2017, 2019; Nachon et al., 2017; Wiens et al., 2017). Table S2 presents APXS elevated concentrations of Mn, Zn, Cu, and Co up to sol 2301 as taken from Berger et al. (2020) APXS compilation, Berger et al. (2017), VanBommel et al. (2019), and from the Planetary Data Scientist (PDS, [https://pds-geosciences.wustl.edu/msl/msl-m-apxs-4\\_5-rdr-v1/mslapx\\_1xxx/extras/](https://pds-geosciences.wustl.edu/msl/msl-m-apxs-4_5-rdr-v1/mslapx_1xxx/extras/)). Table 2 and 3 are simplified versions of Table S1 and S2, respectively, presenting the highest concentrations of transition metals in each formation of Gale crater. Anomalously high metal concentrations in some formations discussed in the following sections might not always be reported in Tables 2-3 and S1-S2 since not available in details in the literature yet. Note that Cr is detected via ChemCam LIBS analyses but no quantification has been established yet, precluding the detection of elevated Cr values throughout the traverse. APXS Cr values are all lower than three times the average crust abundance.

## 2-2. Geologic Context of Gale Crater

Gale crater, with an estimated age of 3.8-3.5 Ga (Laetitia Le Deit et al., 2013; Thomson et al., 2011), hosts record of an ancient lake that was fed by streams and groundwater. Its center comprises a ~5 km thick sedimentary mound named Aeolis Mons, informally called Mount Sharp (John P. Grotzinger et al., 2012). The transition from a wet to dry climate suggested by (Bibring et al., 2006) is strengthened by Gale crater geological record as observed from orbit. Hyperspectral observations acquired by CRISM indicate a transition from Fe-Mg smectites at the lowest portion of the central mound corresponding to the Noachian-Hesperian boundary time to subsequent hydrated sulfate layers and anhydrous minerals at the uppermost strata (Milliken et al., 2010). Rover observations has highlighted a piece of Gale crater geological history that is not visible from orbit. Diagenetic fluids have circulated through Gale crater bedrock, leaving behind phyllosilicates (Vaniman et al., 2014) and a variety of precipitated and diagenetic features like nodules (e.g., Siebach et al., 2014; Stack et al., 2014; McLennan et al., 2014). Subsequent diagenetic fluid circulation and evaporation led to the formation of various salt-filled veins and fractures (e.g., (J. P. Grotzinger et al., 2015; Lanza et al., 2016; Nachon et al., 2014; Rapin et al., 2019). A regolith consisting in modern soil covering the surface of rocks is unevenly deposited throughout Gale crater. Within each of the formation and member presented below, some transition metals are particularly concentrated, either within the bedrock or within diagenetic features.

After landing within the Bradbury formation (Fig. 2), the *Curiosity* rover first drove through sedimentary bedrock composed of sandstones and conglomerates, recording an ancient fluvio-deltaic environment (J. P. Grotzinger et al., 2015). The sedimentary rocks are mostly basaltic in composition (e.g., Rampe et al., 2020) and contain Mg-Fe-clay minerals. Detrital pyroxene and plagioclase grains are present in most of the Bradbury sedimentary rocks, suggesting relatively minimal weathering prior to or during fluvial transport (e.g., Vaniman et al., 2014). Streams transported and deposited sediments including igneous minerals that cemented at the current location. The main provenance of these sedimentary rocks is attributed to a basaltic unit, likely located within Gale crater watershed along the northwestern crater rim (L. Le Deit et al., 2016; McLennan et al., 2014; Siebach et al., 2017). Elevated potassium contents in a few sedimentary rocks (e.g., Anderson et al., 2015) pointed out a potential diversity in the provenance, which was confirmed at the Kimberley formation (Fig. 2) where the CheMin XRD measurements detected sanidine within a drilled K-rich sandstone named Windjana (Fig. 2; Treiman et al., 2016). This discovery, along with the analyses of additional K-rich sedimentary rocks at Kimberley as measured by APXS and ChemCam, suggest a trachytic provenance likely located within the Gale crater watershed too (L. Le Deit et al., 2016; Treiman et al., 2016). Although the disordered nature of sanidine within the Windjana sandstone might support a hydrothermal origin (Morris et al., 2020), the occurrence of float felsic rocks including trachytes (Sautter et al., 2015; Cousin et al., 2017), supports the evolved igneous ( $\text{SiO}_2 > 55$  wt. %) origin (V. Payré et al., 2020). With porphyric feldspar up to 2 cm long, trachy-andesitic and trachytic rocks could be the origin of the detrital feldspar observed within sedimentary rocks (Treiman et al., 2016). Cu- and Zn-rich sandstones with concentrations up to Cu = 1,100 ppm and Zn = 8.4 wt.% (Table 2 and S1; Lasue et al., 2016; Payré et al., 2019) and Mn- Ni- Cu- Zn-rich diagenetic fracture fills (up to MnO = 14.5 wt.%, Ni = 1,000 ppm, Cu = 530 ppm, and Zn = 1.5 wt. %; Table 2-S1; Lasue et al., 2016; Lanza et al., 2016; Payré et al., 2019) cutting through the Kimberley sandstones were measured by both LIBS and APXS and highlight the lithologic diversity explored within this geologic unit.

Driving further, the *Curiosity* rover reached the lacustrine mudstones of the Murray formation (Fig. 2) forming the first several hundred meters of the Mount Sharp group and evidencing an ancient lake. Some of the Murray sedimentary rocks are covered by the Stimson formation, which comprises eolian sandstones unconformably lying above both the Murray and Bradbury formations (Banham et al., 2018). Pahrump Hills, the lowermost member of the Murray formation, exhibits laminated mudstones that sometimes present Ni- and S-enriched diagenetic aggregates (Ni > 625 ppm; Table 2-S1; Nachon et al., 2017). At the Garden City



outcrop located at the bottom of the Pahrump Hills member (Fig. 2), the *Curiosity* rover discovered a mudstone outcrop widely crosscut by a prominent assemblage of diagenetic light-toned and dark-toned veins sometimes associated with Ge, Mn, and Zn enrichments (up to Ge = 650 ppm, MnO = 1 wt. %, and Zn = 2,400 ppm; Fig. 4; Table 2-3 and S1-S2; Berger et al., 2017).

Traveling up-section within the Murray formation, the rover reached the Sutton Island member. It consists of heterolithic mudstones and sandstones, which are thought to have been deposited within a marginal lake setting (Fig. 2; Grotzinger et al., 2015; Stein et al., 2018). Located stratigraphically just above Sutton Island, the Blunts Point member exhibits thinly laminated mudstone, likely deposited in a lacustrine environment (e.g., Sun et al., 2019). Near the contact between the two members, Mn-rich signatures have been measured in both diagenetic nodules and sandstones with MnO concentrations up to 16 wt. % (Gasda et al., 2019). Stratigraphically above Blunts Point, the Pettegrove point and the lower portion of the Jura member are part of the Vera Rubin Ridge (VRR) topographic feature (Fig. 2), which is known to exhibit significant hematite signatures according to orbital spectral observations. Bleached halos in portions of the VRR are associated with low MnO concentrations (< 0.25 wt.%; L'Haridon et al., 2020). Deposited in a lacustrine environment, a series of diagenetic events through groundwater circulation hardened the VRR mudstones compared to the surrounding Murray rocks (Fraeman et al., 2020; Frydenvang et al., 2020). *Curiosity* then arrived at a major mission destination in early 2019 at the clay-bearing unit, also known as Glen Torridon (Fig. 2), which is part of the Jura member of the Murray formation. There the rover encountered lacustrine finely laminated Mg-rich mudstones with elevated Cu, Zn, and Mn concentrations (e.g., (W. Goetz et al., 2020). The Greenheugh pediment, located just above Glen Torridon as a capping unit, are eolian sandstones that are part of the Siccar Point group (Fig. 2), unconformably resting on some members of the Mount Sharp sedimentary rocks (Bryk et al., 2019). As of this writing, the rover left Glen Torridon.

High abundances of transition metals measured within Gale crater bedrock and diagenetic features can be explained by the occurrence of metal-bearing minerals like chalcopyrite for Cu or their adsorption at the surface of oxides. Based on terrestrial settings, possible processes that could explain high metal abundances include magmatic processes potentially associated with hydrothermal circulation, erosion of parental rocks and transportation of the eroded products through streams, subsequent sorting processes, and/or diagenetic fluids (e.g., Farrow and

Watkinson, 1992; Cox et al., 2003). The following sections will review the current proposed ideas to explain the origin of those metal deposits.

### **3. Gale Crater: a Storage Basin for Metal-Rich Sediments**

#### **3-1. A Metal Deposit in Gale Crater's Vicinity**

At the Kimberley formation, potassic sandstones exhibit elevated Cu, Zn, and Ge concentrations. Sandstones contain detrital pyroxene, plagioclase, and sanidine, which have been interpreted as coming from at least two provenances of basaltic and trachytic origin (L. Le Deit et al., 2016; V. Payré et al., 2020; Treiman et al., 2016). Sub-millimetric analyses by ChemCam of the sandstones containing elevated Cu concentrations (100 – 1,100 ppm) revealed that Cu, likely associated with sulfur as a potential chalcopyrite form, is mainly found with detrital igneous minerals including alkali feldspar (Payré et al., 2019). Such an association suggests that Cu-bearing minerals likely originated from the same trachytic provenance of detrital minerals of the Kimberley formation. LIBS measurements with Cu concentrations up to 1,000 ppm occur in association with feldspar-like compositions in a porphyritic trachy-andesite rock further support a magmatic origin (Payré et al., 2019). Because Cu, Ge, and Zn can be concentrated by high-temperature fluids (>150°C) and can be drastically partitioned in low-temperature fluids, the co-occurrence of elevated concentrations of Cu, Ge, and Zn within potassic sandstone analyzed by both ChemCam and APXS (Cu = 600 ppm, Ge = 250 ppm, and Zn = 900 ppm; Table S1-S2) at the Kimberley formation suggests a hydrothermal origin at the igneous provenance (Berger et al., 2017; Payré et al., 2019). No mineral specific to hydrothermal alteration such as zeolite and amphibole has been observed in any of the rocks analyzed in Gale crater so far, thus suggesting that the hydrothermal circulation was centered at the source region of transition metals and detrital minerals within the Gale crater watershed (Berger et al., 2017; Payré et al., 2019). Unlike Cu, Zn is not associated with sulfur and could either be incorporated in phyllosilicates such as saucornite or be present as zinc oxides (Lasue et al., 2016).

Although additional scenarios might explain Cu concentrations in the Kimberley sandstones, three main possible mechanisms are envisioned (Payré et al., 2019). (1) Hydrothermal circulation of potential S-bearing fluids within an evolved magmatic body located in the watershed of Gale crater could have accumulated Cu in sulfide minerals, which could have been then incorporated into some felsic rocks after cooling, accumulated in hydrothermal veins, and disseminated in the rocks surrounding the magmatic complex as

observed on Earth (e.g., Sillitoe, 2010). Following the erosion of the resulting igneous outcrop, and fluvial transport of eroded products, the sediments would have been deposited and cemented at the current location in the Kimberley formation. (2) Hydrothermal fluids generated by the substantial heat related to an impact in the vicinity of Gale crater, as observed in Sudbury crater, Ontario, Canada (e.g., Ames et al., 2008), could have mobilized transition metals from crater-floor rocks and crystallized metal minerals associated with minerals from a differentiated impact melt. Similarly to (1), after melt cooling, erosion of the outcrop and transportation of the products through streams up to the Kimberley formation could explain the accumulation of Cu in the potassic sandstones. (3) As commonly observed on Earth, fumarole circulation through rocks could have sublimated transition metals located in the host rocks, forming a metal deposit within the watershed. In any scenario, hydrothermal circulation likely concentrated Cu as potential sulfides in felsic igneous rocks, sometimes associated with feldspar. The co-occurrence of elevated Cu and Zn concentrations in several potassic sandstones suggest a similar origin. Yet, the absence of Zn-sulfides has been attributed to supergene weathering (Lasue et al., 2016), with the leaching of sulfur deposits enriched in Zn, the secondary products potentially being transported to the Kimberley formation and deposited in pores and fractures. Such sulfur deposit might correspond to the Cu-deposit, although Zn-sulfides would be expected in the Kimberley sandstones as inferred for Cu-S minerals. Two scenarios are hence envisioned. (1) Oxidizing fluids as commonly observed on Earth could have leached Zn from a sulfide deposit also containing Cu-S minerals like chalcopyrite (Hitzman et al., 2003). Such fluids would replace Fe-Cu-sulfides to Fe and Cu oxides and Cu-S minerals like chalcocite. The concurrent and/or subsequent fluvial erosion of the metal deposit could have led to the transportation of Cu-bearing felsic rocks and potential additional Cu-S minerals up to Gale crater. (2) The occurrence of at least two metal deposits, one Cu- and one Zn- sulfur deposits, in Gale crater's catchment can also be envisioned. In all possible scenarios, such high concentrations of Cu and Zn within the Kimberley sandstones reveal evidence for the first metal ore-like deposits ever observed on Mars.

### 3-2. Accumulation of Transition Metals through Depositional Processes

Various locations in Gale crater present anomalously high transition metal concentrations, while not necessarily related to hydrothermal circulation. Lacustrine sandstones located at the transition between the Sutton Island and Blunts Point member, and the fluvio-lacustrine mudstones from the Jura member in the Glen Torridon unit (Fig. 2), both display elevated transition metal concentrations that are likely associated respectively with the precipitation of

metal-bearing oxides from oxidizing lake waters and with sorting processes. Fracture fills in the Kimberley formation, diagenetic aggregates and nodules at Pahrump Hills, and a prominent vein network in the Garden City outcrop all contain elevated transition metal concentrations (Fig. 2), likely related to diagenetic fluid circulation that postdates lithification of bedrock. These observations are discussed below.

#### *Metal-oxide precipitation from stream and lake waters*

Several sandstones from the Yellowknife Bay and Bradbury formations present elevated MnO concentrations up to 16 wt. % (Table 2), likely concentrated within oxidized Mn-rich minerals like birnessite (Lanza et al., 2014). Most of them being integrated within grains of sedimentary rocks, Lanza et al. (2014) interpreted such enrichments as either the transportation of Mn-rich minerals from Gale crater's catchments or authigenic phases. In any case, the precipitation of Mn is related to a highly oxidizing environment. At the transition between the marginal lake setting at Sutton Island and the lacustrine setting at Blunts Points, additional manganese enrichments from 1.5 wt. % to 16.0 wt. % of MnO have been measured by ChemCam within light- and dark-toned lacustrine sandstones (Gasda et al., 2019). Because elevated Mn concentrations are observed within sandstones from both Sutton Island and Blunts Point, Gasda et al. (2019) suggests precipitation of Mn-oxides from a shallow high-energy oxidizing water environment 3.6-3.2 Gyr ago (J. P. Grotzinger et al., 2015; Hurowitz et al., 2017; Stein et al., 2018), above the oxic-anoxic limit. Groundwater fluids circulating through lake-floor sediments could have accumulated  $\text{Mn}^{2+}$  cations. Note that localized Mn-rich nodules in the area are likely the result of diagenetic fluid circulation following the lithification of the sandstones (Gasda et al., 2019; Meslin et al., 2018). The precipitation of Mn-oxides from lake waters highlights the necessity of a powerful oxidant that enables the oxidation of Mn (potential redox  $E_h \gg 500$  mV). This oxidant could have possibly been perchlorate, chlorate, or oxygen; the action of such oxidants contributes to a necessary condition (a readily available energy source) for the habitability of Mars.

#### *Sorting processes during stream transport*

Coherent fine-grained lacustrine mudstones from the Jura member located within the Glen Torridon unit (Fig. 2) display elevated Mn, Zn, and Cu associated with high MgO and low  $\text{K}_2\text{O}$  contents compared to the surrounding Zn- Mn- Cu- depleted rubbly coarse-grained mudstones (W. Goetz et al., 2020; O'Connell-Cooper et al., 2020; Thompson et al., 2020). The fine-grained thinly laminated mudstones containing elevated transition metal concentrations suggest a

lacustrine origin from a low-energy environment, while the cross-laminated coarse-grained mudstones depleted in transition metals support a lacustrine origin from a relatively higher energy environment (Rampe et al., 2020). Although the composition and mineralogy of Glen Torridon bedrock compared to the hematite-rich Vera Rubin Ridge suggest a limited diagenesis within the Glen Torridon unit (Fox et al., 2020), the addition of Mn, Zn, and Cu to the Mg-rich mudstones after lithification through diagenetic fluid circulation could be envisioned (Thompson et al., 2020). Because Mn, Zn, Cu, and Mg enhancement is exclusively associated with fine-grained mudstones, sorting processes during stream transport might also explain the accumulation of transition metals in the Jura member (O'Connell-Cooper et al., 2020). Sorting process is also evidenced by the detection of a higher amount of pyroxene grains and a lower amount of light feldspar within two samples analyzed by CheMin within the Mg-rich fine-grained mudstones compared to those detected within the coarse-grained rubbly K-rich mudstones (Thorpe et al., 2020). Although no clear conclusion is drawn at the writing time of this paper, Mn, Zn, and Cu enhancement observed within the Mg-rich mudstones might be related to sorting during stream transport with transition metals potentially coming from the same basaltic provenance as pyroxene. A thorough study and review of the metal-rich mudstones from the Glen Torridon area is needed to constrain the most likely process.

#### *Diagenetic processes*

Following the deposition and lithification of sandstones and mudstones, diagenetic fluids likely precipitated or deposited metal-bearing minerals in various features including fractures and veins. To date, the Kimberley formation is one of the locations in Gale crater concentrating the highest abundances of transition metals ever measured by the *Curiosity* rover. In addition to the sandstones discussed in the previous section, resistant fracture fills (represented by the Stephen, Neil, and Mondooma targets) cross-cutting the Kimberley sandstones next to the Windjana site (Figs. 2-3) present unexpected elevated concentrations of MnO, Co, Ni, Cu, and Zn, which are well above those observed within the surrounding bedrock. APXS and ChemCam measured MnO = 3.0-14.5 wt. % (Berger et al., 2017; Lanza et al., 2016; Table 2-3 and S1-S2), Co ~ 300 ppm (VanBommel et al., 2017; Table 3), Ni = 1,287 ppm (Berger et al., 2017; Table 3), Cu up to 530 ppm (Payré et al., 2019; Table 2), and Zn = 8,490 ppm according to APXS (Berger et al., 2017; VanBommel et al., 2017; Table 3) and up to ZnO = 2.8 wt. % according to ChemCam (Lasue et al., 2016; Table 2) in the fracture fills. The lack of correlation between MnO and S, C, and Cl argues against Mn- sulfur, carbonate, or chloride phases but rather suggests the existence of Mn-oxides (Lanza et al., 2016a). The low optical reflectance values

of the fracture fills match those obtained in laboratory on Mn-oxides, supporting the occurrence of Mn-oxide minerals (Fox et al., 2015; Hardgrove et al., 2015). The absence of elevated MnO concentrations within the surrounding bedrock suggests that following the deposition and cementation of the Kimberley sandstones, fracturing occurred and an oxidized Mn-rich fluid circulated precipitating a thin layer of Mn-oxides (Lanza et al., 2016a). Furthermore, because no enrichment of MnO is observed within any Kimberley sedimentary bedrock, the source of Mn is likely distant from the Kimberley formation (Lanza et al., 2016a). The sandstones were deposited and cemented in early Hesperian (<3.5 Gyr), so the emplacement of the Mn-fracture fills was more recent than 3.5 Gyr ago. The positive correlations between MnO and most of the transition metals suggest an association of Ni, Zn, and Cu with Mn-oxides. As commonly observed on Earth (e.g., Della Puppa et al., 2013), Ni, Zn, and Cu have been likely adsorbed on Mn-oxides through the circulation of the Mn- bearing oxidizing fluid or a subsequent one, which supports a source of oxygen on Mars, potentially being the atmosphere (Lanza et al., 2016; Lasue et al., 2016; Payré et al., 2019).

At Pahrump Hills (Fig. 2), clusters and dendritic aggregates contain elevated Ni contents (Ni > 625 ppm; Nachon et al., 2017; Table 2 and S1). Aggregates are embedded in mudstones and likely formed by magnesium sulfates. Because the aggregates cross-cut the laminations of the host bedrock and are embedded within the mudstones without noticeable boundaries, the Ni-bearing aggregates likely grew through early diagenetic fluid circulation within the laminated mudstones' pore space during cementation (Nachon et al., 2017a).

At Garden City (Figs. 2 and 4), 1-6 cm-thick dark veins composed of CaO, SiO<sub>2</sub>, and FeO contain moderate MnO (1.0 wt. %) contents, and elevated Zn (2,472 ppm) and Ge (650 ppm) concentrations compared to the cross-cut host rock (Berger et al., 2017; Table 3 and S2). The detection of a fluorine peak within LIBS spectra (Forni et al., 2015; Nachon et al., 2017a) supports the circulation of a diagenetic F-bearing fluid that mobilized Mn, Ge, and Zn and precipitated them within Garden City veins (Berger et al., 2017). The analyses of variable compositions within the dark-toned veins suggest a complex fluid circulation history, with either fluids with various compositions or several episodes of formation.

In summary, at least one metal (Cu and/or Zn) deposit located in Gale crater's watershed was formed by hydrothermal fluids either exsolved from a magma or impact-related that mobilized transition metals from an evolved magma. Subsequent streams leached transition metals including Zn from the deposit, eroded and transported elements and minerals into the lake. Cu-sulfides and Zn non-sulfide minerals were deposited within sediments that were later

lithified. Groundwater circulation through sediments on the lake-floor could have concentrated Mn, then precipitating as Mn-oxides within the shallow lake oxic waters. Because each metal is soluble under different conditions (e.g., pH and redox of water), various episodes of diagenetic fluids then mobilized and re-mobilized metals from one or several unknown regions and deposited them as oxide, sulfide, sulfate, or silicate within fractures, veins, and aggregates. Such process is well-illustrated by the interpretation of multiple diagenetic events at Vera Rubin ridge, which mobilized and remobilized redox-sensitive metals including Mn within reducing fluids during late-stages of diagenesis, releasing Mn from the hematite-bearing VRR mudstone (L'Haridon et al., 2020). Although all transition metals might come from the same deposit, several metal sources could be envisioned since the mobility and affinity of each metal is distinct from one another. Overall, the MSL mission points out that metal deposits do exist on Mars and can be readily identified on the ground while challenging to detect from orbit certainly due to their small size, the absence of specific spectral features, and/or the dust cover, suggesting that metal deposits might be more common than previously thought.

### 3-3. Extra-Martian Metal Carriers

In addition to endogenous origins, transition metals are also supplied to Mars through meteoritic impacts. To date, the *Curiosity* rover has analyzed tens of distinguishable dark and smooth meteorites with ChemCam and Mastcam (Fig. 5; Table 2 and S1; Johnson et al., 2021, 2020). Reflectance spectroscopic analyses acquired by the Mastcam instrument onboard the *Curiosity* rover revealed pristine iron meteorites, and LIBS analyses confirmed their Fe-rich nature (Fig. 5c-d), as well as the presence of elevated Ni up to 21.2 wt. % (Table 2 and S1; (Johnson et al., 2020, 2021). APXS measurements on one iron meteorite Gretna\_Green support elevated Ni concentrations (2,623 ppm, Table 3). Nickel is commonly observed in high abundances in Fe-meteorites due to its strong affinity with Fe as an alloy. Comparing LIBS spectra from iron meteorites analyzed on Mars and in the lab within a martian chamber ( $P_{CO_2} \sim 6$  mbar), several iron meteorites discovered in Gale crater display spectra similar to the Fe-Ni alloy kamacite, supporting the occurrence of such a mineral within these meteorites, as commonly observed in iron meteorites found on Earth (Meslin et al., 2019; R. C. Wiens et al., 2017). The unexpectedly high amounts of Ni compared to most iron meteorites found on Earth indicate that some of the iron meteorites found in Gale crater might be ataxites, which are very rare on Earth. In addition, the elevated abundances of Ni and P within the Egg Rock meteorite suggest the presence of schreibersite  $(Fe,Ni)_3P$  (R. C. Wiens et al., 2017).

In addition to iron meteorites, potential chondrites have also been analyzed by ChemCam. Comparing with terrestrial meteorite collections, which consist of a majority (> 70%) of chondrites, at least 150 chondrites are expected to have been imaged and/or analyzed by the rover (Lasue et al., 2019; Meslin et al., 2019). However, the detection of such meteorites is challenging due to their textures, which can be difficult to distinguish from dark smooth rocks like basalts, and due to potentially higher weathering rates than iron meteorites. As observed on Earth, chondrites contain high Ni contents (> 1.0 wt. %), elevated MgO concentrations (MgO = 20-30 wt. %), and a Ni-Mg ratio inconsistent with that measured in typical Mars rocks. Based on these criteria, at least two cm-size pebbles and one float rock measured by ChemCam are good candidates to be chondrites (Lasue et al., 2019, 2020).

With several tens to tens of thousands grams of chondrites (Lasue et al., 2019) and up to 800 iron meteorites/km<sup>2</sup> along the rover path only (Meslin et al., 2019), meteorites are a compelling supplier of various metals, especially Ni, and are a valuable source of transition metals at the surface of Mars. According to the average of Ni concentrations within soils measured by the *Spirit* rover (Ni = 237-679 ppm), (Yen et al., 2006) suggests a meteoritic contributions around 1% to 3%. Because the relative timing between these meteorite impacts and the diagenetic circulation within various sedimentary formations in Gale crater is currently unknown, it is hard to estimate whether iron meteorites and chondrites could be sources of some of the Ni enhancements observed in a few locations in Gale crater, like the Pahrump Hills aggregates. The rate and amount of metal input at the surface of Mars from meteorites is also difficult to assess since the rate of falls cannot be estimated, mainly due to an unknown erosion rate of meteorites on Mars.

#### **4. To What Extent Do Transition Metals Occur at the Surface of Mars?**

On Earth, different types of metal deposits exist, including those that are within or in contact with igneous rocks with minerals transported and/or crystallized from a magma (magmatic), those that are located within and/or in contact with igneous rocks with minerals precipitating from hydrothermal circulation (hydrothermal), and hydrothermal deposits with hydrothermal fluids derived from a magma (magmatic-hydrothermal). Metal deposits formed within a sedimentary environment also exist as the result of mineral precipitation from surface waters or accumulation of minerals after transport and deposition.



As highlighted in Gale crater, much of the surface of Mars has experienced complex surface and hydrothermal fluid circulation that concentrates transition metals released from igneous and sedimentary outcrops by water alteration. In addition to such processes that could precipitate and accumulate metals within sedimentary deposits, Mars' magmatism likely contributed to the formation of metal deposits. Mars' magmatism is mainly basaltic as inferred from martian meteorites (e.g. Udry et al., 2020) and rover and orbital measurements of the surface. Most magmatic metal deposits found on Earth are in association with mafic and ultramafic settings. Depending on the affinity of each metal with a silicate melt, some elements tend to accumulate early in mafic magmas (compatible elements, e.g., Ni) while others are concentrated in more differentiated melts (incompatible elements, e.g., Mo, Au; Ridley, 2013). As an example of a magmatic deposit, compatible elements can be concentrated during fractional crystallization within a shallow magma chamber, forming metal-bearing minerals like chromite, which sink to the bottom of the chamber together with silicate minerals. Such a process can result in disseminated metal-bearing minerals like chromite throughout the resulting mafic and ultramafic cumulates (Ridley, 2013; and references therein). Another magmatic setting is related to the well-known Ni-Cu sulfide and Platinum-Group Element (PGE) deposits. Elevated sulfide mineral concentrations within a silicate melt can result in the formation of two immiscible magmas when sulfide saturation is reached, one being a sulfide melt and the other a silicate melt. Transition metals that show a stronger affinity to sulfide melts than to silicate magmas (chalcophile elements, e.g., Cu, Zn, Ni, Pt) will be concentrated within the sulfide melts (Ridley, 2013; and references therein). Because Cu, Ni, and PGEs are compatible within mafic and ultramafic melts, sulfide magmas will become enriched in those chalcophile elements, forming the well-known PGE deposits. Magmatic-hydrothermal deposits, the polymetallic Volcanic-Hosted Massive Sulfide (VHMS) deposits (mainly Cu, Zn, Pb, Au, and Ag), are found on the oceanic seafloor where hydrothermal vents release fluids from the oceanic crust into the seawater in the vicinity of the mid-ocean ridges, arc, back-arc and marginal basins (Ridley, 2013; and references therein).

Although all terrestrial conditions allowing the formation of such deposits might not be met on Mars, such as a specific oxygen fugacity or particular tectonic setting, comparable deposits encountered in mafic and ultramafic rocks might be found on Mars. Evidence of martian fractional crystallization was identified some time ago based on surface exploration with the *Spirit* rover in Gusev crater (McSween et al., 2006; V. Payré et al., 2020; Sautter et al., 2015; Arya Udry et al., 2018), and on a ~4.1 Ga martian meteorite named Allan Hills (ALH) 84001 identified as an orthopyroxene cumulate (Lapen et al., 2010), suggesting the potential existence

of metal-deposits related to the differentiation of magmas. Elevated sulfur concentrations at the surface of Mars and within martian meteorites (e.g., Gaillard and Scaillet, 2009; King and McLennan, 2010; and references therein) suggest that the mantle and the crust are sulfur-rich, potentially favoring the formation of immiscible melts, although they have not been identified yet (King & McSween, 2005). Chalcophile sulfide deposits might therefore occur. Evidence of hydrothermal circulation through crustal mafic rocks has been observed in Gusev and Gale craters (Berger et al., 2017; Ruff & Farmer, 2016), not to mention the widespread hydrothermal circulation related to impacts (Abramov & Kring, 2005; Schwenzer et al., 2012), suggesting the possibility of concentrating transition metals by hydrothermal fluids. The existence of metal deposits associated with mafic rocks on Mars is therefore highly probable.

The remarkable evidence of intermediate to felsic magmatism on Mars additionally expands the types of metal deposits that could be found. Most hydrothermal-magmatic deposits are associated with intermediate to felsic crustal volcanism (Ridley, 2013). The decrease of solubility of water and other volatile elements contained within intermediate to felsic magmas when ascending through the crust results in the exsolution of the volatile species and the formation of hydrothermal fluids. Metals that do not display a strong affinity with the crystallizing minerals and are soluble in the fluid will be partitioned into the hydrothermal fluids. For instance, if Cu behaves as an incompatible element with the crystallizing minerals, its high solubility behavior with the fluids will lead to its concentration within the hydrothermal solution rather than the silicate melt. If Cu is compatible with a crystallizing phase, it will be less concentrated in the solution. Terrestrial hydrothermal-magmatic metal deposits are numerous and include porphyry deposits, being commonly enriched in copper, gold, and molybdenum, as well as related elements. Most of these metal deposits are located in arc and back-arc settings, especially due to the elevated water contents released from the subducted tectonic plates ( $\text{H}_2\text{O} > 4.0 \text{ wt.}\%$ ; e.g., Richards, 2009; Ridley, 2013) and the elevated oxidation state of the magmas. Although several studies suggest high oxygen fugacity  $f\text{O}_2$  in the martian crust and upper mantle  $> 3.7 \text{ Gyr}$  ago (up to 3 log unit above the fayalite-magnetite-quartz FMQ buffer; e.g., McCubbin et al., 2016a; Santos et al., 2015; Tuff et al., 2013) and water contents exceeding 1.0 wt. % in Noachian crustal magmas (e.g., McCubbin et al., 2016b; Stolper et al., 2013), these two parameters are tricky to constrain on Mars. Exploring Mars' magmatic history is therefore essential to evaluate the type of metal deposits that could have formed on Mars. Precious metal deposits might exist, and it is highly probable that future missions with additional sophisticated instruments will discover such settings according to the existence of

felsic magmas and high  $fO_2$  and hydrated melts from the Noachian period. At the surface of Mars, felsic terrains are localized in tens of locations according to orbital measurements and perhaps extend to a large portion of the subsurface, as suggested in Sautter et al. (2016). The only felsic rocks measured by rovers have so far been found in Gale crater and Ares Vallis by the *Sojourner* rover although the Si-rich rocks measured by the latter might be sedimentary (Foley et al., 2003; McSween et al., 1999). In Gale crater, elevated Cu concentrations were sometimes associated with felsic rocks including a porphyritic trachy-andesite. These were hypothesized to have come from a hydrothermal region, suggesting a magmatic-hydrothermal or hydrothermal Cu-deposit at the source (Payré et al., 2019). Although this observation might be localized, current and future rover missions like the Mars 2020 *Perseverance* mission will provide additional insights into the extent of such deposits at the surface of Mars.

The Mars 2020 *Perseverance* rover successfully landed in Jezero crater within a  $> 3.8$  Gyr old terrain on February 18<sup>th</sup>, 2021 (Fig.1). Igneous rocks and sedimentary rocks rich in igneous minerals are expected to be found, since the rover landed in the vicinity of the terminus of a large delta that appears to have collected materials from a spectacular diversity of sedimentary and volcanic terrains (Goudge et al., 2015). Most of the materials concentrated by the delta, and the materials in the regions surrounding Jezero crater, appear from orbit to be mafic and weathered mafic materials (e.g., Ehlmann and Mustard, 2012; Horgan et al., 2020). The Mars community may not have the opportunity to sample felsic products and byproducts as it has done in Gale crater, but will likely observe a sequence of weathering from mafic olivines to serpentines and carbonates. Yet, surface exploration often brings surprises not seen from orbit. The SuperCam instrument (Maurice et al., 2021; Roger C. Wiens et al., 2020), which is an upgraded version of ChemCam, is able to rapidly measure at a distance the concentrations of a set of transition metals (Mn, Cr, Ni, Zn, and Cu) using LIBS. The PIXL instrument allows the team to map a large range of elemental abundances including metals (V, Cr, Mn, Co, Ni, Cu, Zn, Y, and Zr) for rocks of interest through X-ray Fluorescence (Allwood et al., 2020). The Mars 2020 mission kicks off the first sample return mission aiming to send sedimentary and volcanic samples of interest back to Earth in a series of three connected missions. The most sophisticated analyses of the martian samples will be then possible, providing fundamental information regarding the geology and the habitability of Mars and preparing for future human exploration. The Mars 2020 payload will certainly enlighten us on the distribution of metals including transition ones at the surface of Mars and its interior, and help us to evaluate the extent of metal deposits related to mafic and perhaps felsic volcanic outcrops. The outcomes

will serve both the geology and astrobiology studies of Mars, and will help ensure the safety and well-being of the future astronauts when they eventually explore the surface of Mars.

## **5. Perspectives on the Importance of Transition Metals for Life and Human Exploration**

### **5-1. Essential Resource for Life Development and Sustainability**

On Earth, one of the fundamental resources required for emergence and sustainability of life as we know it is liquid water, which acts as a medium that facilitates biochemical reactions and nutrient transport. On Mars, the past circulation of liquid water is illustrated by a multitude of evidences, including geomorphologic traces of ancient rivers, deltas, alluvial fans, and paleo-lakes, and the occurrence of water-bearing minerals such as phyllosilicates that attest to surface and near-surface aqueous activity (e.g., Bibring et al., 2006; Carr and Head, 2015; Ehlmann et al., 2011; Grotzinger et al., 2015; Lapotre et al., 2016). Yet, liquid water alone is not sufficient to allow the emergence of life (e.g., Knoll and Grotzinger, 2006). All known living systems also require sources of key chemical elements. In addition to the so-called CHNOPS elements (carbon, hydrogen, nitrogen, oxygen, phosphorus, and sulfur) that are vital for the synthesis of the basic macromolecules of living systems, metals including transition metals are essential for the survival of micro-organisms as well as for humans (e.g., Hughes and Poole, 1989; Gadd, 1992). An extensive overview of the importance of metals in the origin of life is provided in Clark et al. (2021), and examples are presented below.

In trace amounts, transition metals are responsible for the functioning of an organism by performing various roles in cells. In addition to stabilizing cellular structures such as cell walls and membranes, up to one third of all known enzymes need at least one transition metal as a functional participant (Hoppert, 2011). Enzymes are proteins that accelerate chemical reactions in organisms. For instance, the enzyme called superoxide dismutase helps to break down dangerous oxygen molecules called “superoxides” in cells, preventing potential diseases (e.g., Pittman, 2005). Transport processes for cell functioning, oxidation, and nutrition occur through membranes, and metals play a key role creating charge and concentration gradients across membranes that allow intra- and inter-cellular exchanges and communications between the environment and cells (e.g., Hughes and Poole, 1989). To cite Gadd (1992), “[for microorganisms], metals are directly and/or indirectly involved in all aspects of growth, metabolism and differentiation” and “deprivation of an essential metal ion will, by definition,

ultimately result in death.” The lack of metals including transition metals availability at the surface of a planetary body would thus be detrimental to the formation and evolution of living organisms, and an excess of metals would become toxic.

A remarkable example of how transition metals played a key role in the origin of life is carbon fixation, which is a critical process for some organisms to produce complex organic molecules essential for biosynthesis such as cellular architecture. Several pathways allow such a biochemical process, but the most primitive and efficient way is through the acetyl-CoA pathway, i.e., Wood-Ljungdahl (Cotton et al., 2018; Ragsdale, 1991). Transition metal-bearing molecules including Co(III) are involved within the reaction sequence, making transition metals of significant importance for biosynthesis. Before the existence of complex proteins currently involved as catalyzers in Wood-Ljungdahl pathway, Varma et al. (2018)’s chemical experiments suggest that CO<sub>2</sub> fixation in a similar fashion could have occurred with native transition metals as catalyzers, like Ni<sup>0</sup> and Co<sup>0</sup>. Carbon building blocks similar to those formed by the Wood-Ljungdahl pathway could then be produced (e.g., formate, acetate, and pyruvate), supporting the idea that the earliest organisms on Earth might have been able to fix carbon with native metals as catalyzers.

Manganese was central in the rise of dioxygen in the Earth’s atmosphere 2.5 Gyr ago (Fischer et al., 2015). The photosystem II, composed of an essential cluster of Mn<sub>4</sub>CaO<sub>5</sub>, is a protein complex that initiates photosynthesis reactions in microorganisms like cyanobacteria (e.g., Marschner, 1995; Lingappa et al., 2019). Located within the photosynthetic membrane of cells, the photosystem II uses light energy to form high-energy electrons, enabling the oxidation of H<sub>2</sub>O to H<sup>+</sup> and O<sup>2-</sup> outside the cells (lumen; Fig. 6). The released protons then cross the photosynthetic membranes, providing enough energy to form the vital Adenosine-TriPhosphate (ATP) molecules necessary to drive the photosynthetic reactions.

Some transition metals, such as manganese, also play a crucial role in cellular protection against toxic molecules. For instance, superoxidase dismutase (SOD) molecules including the manganese superoxidase dismutase (MnSOD) and the Cu-Zn superoxidase dismutase (Cu-Zn SOD) are antioxidant enzymes present within cells whose function is to maintain a low level of the toxic reactive superoxide O<sub>2</sub><sup>•-</sup> according to the following reaction:  $2\text{O}_2^{\bullet-} + 2\text{H}^+ \rightarrow \text{O}_2 + \text{H}_2\text{O}_2$  (Marschner, 1995; Pittman, 2005; Lingappa et al., 2019; and references therein). Overall, both the importance of Mn in photosynthesis and anti-oxidant properties of transition metals, illustrate how these elements are vital elements in many, if not most, organisms.

Ribonucleic acid (RNA) enables any cells to access to the genetic information necessary for any living organisms. RNA is composed of a sequence of nucleotides formed by a

nucleobase (adenine, cytosine, guanine, or uracil), a sugar called ribose, and a phosphate group. Driven by wet-dry cycles, Becker et al. (2019) show that metals including Cu and Zn could have been catalyzers in the prebiotic synthesis of RNA from pre-existent ribose and nitrogen-bearing molecules along with other key molecules such as urea and salts. Such a process suggests that transition metals played a crucial role in the formation of life's building blocks in prebiotic time on Earth, likely within a hydrothermal vent that would have provided the physiochemical properties needed for RNA synthesis (Becker et al., 2019). Such a geological setting has been suggested to have occurred on Mars (e.g., Michalski et al., 2017; Ruff and Farmer, 2016). Estimating the abundance of transition metals at the surface of Mars is essential to unravel whether complex molecules like RNA could have been synthesized on Mars, opening vital opportunities for life to grow.

## **5-2. Transition Metals and Human Exploration**

Human exploration of space has recently received a lot of attention, particularly the Moon and Mars, which are our close planetary neighbors with compelling geologic histories. As part of the Artemis program implemented in 2020, NASA astronauts are expected to go back to the Moon within a decade, thus taking a step forward towards the human exploration of Mars. Sending humans to Mars is highly motivated by a combination of science, exploration, as well as leadership. In addition to our desire to expand our presence to other planetary bodies, sending humans to Mars is a step towards better understanding another planetary body in our solar system and toward the settling of other planets. A crewed mission, combined with the use of robots, is expected to substantially enhance the efficiency of scientific investigation of Mars' surface (Beaty et al., 2015). From human safety to waste recycling and food production, sustainable systems are crucial to long-term habitation on Mars. In this context, the role of metals including transition metals is critical to understand, as these elements are crucial for sustainable agriculture and waste management, as well as being toxic to human beings.

### **5-2.1. Importance of Metals for Agriculture**

One of the main objectives of public and private space agencies is to minimize re-supply from Earth to reduce mission costs and safety issues (e.g., Bubenheim et al., 1995; Silverstone et al., 2003; Zubrin, 2011). The use of *in situ* resources including water, regolith, and light is thus fundamental to the closed-cycle long-term habitation of Mars. To be viable, food production is essential, starting with the growth of a variety of plants within sheltered

greenhouses to ensure a complete and varied diet for humans. The martian regolith is envisioned to be utilized as a sustainable agricultural soil (Eichler et al., 2021; G. W. W. Wamelink et al., 2019; G. W. W. W. Wamelink et al., 2014). Several seedling experiments have been carried out in a variety of synthetic martian regolith materials (Morris et al., 2000; O’Connell-Cooper et al., 2016; Cannon et al., 2019). These successfully led to the growth of several kinds of plants such as lettuce, arugula, tomatoes, radishes, and quinoa in a terrestrial atmosphere at ambient temperature (Eichler et al., 2021; G. W. W. Wamelink et al., 2019; G. W. W. W. Wamelink et al., 2014). The addition of fertilizers are still essential for an optimum growth of plants as demonstrated by Eichler et al., (2021). In trace but critical amounts, Cr, Mn, Ni, Cu, and Zn, are required for plant growth, development, and productivity (Alloway, 2013; Eichler et al., 2021; and references therein). Deficiency in metals like transition metals might cause irreversible physiological stress to plants, induce a reduction in growth rate and yield and, in extreme cases, crop failure (see Alloway, 2013 for detailed symptoms of micronutrient deficiencies in plants). At optimal concentrations, crucial roles of these metals include aiding optimal functioning of enzymes and photosynthesis, atomic gradients in intra- and extra-cellular space, and cellular protection as presented in Section 3.1 (e.g., Alloway, 2013; Arif et al., 2016). The martian regolith simulants used for seedling experiments did not consider the trace metal concentrations measured in soils by recent missions such as Cr, Mn, Ni, Cu, and Zn. Instead of adding resource-expensive Earth-supplied fertilizers to facilitate food production, the martian regolith may therefore be surprisingly productive if the regolith simulants are sufficiently relevant. On the other hand, excessive concentrations of transition metals might be lethal for plants. For example, Mn at > 200-300  $\mu\text{mol/L}$  causes necrotic lesions on soybean leaves (Santos et al., 2017). Estimating the concentration and distribution of transition metals at the surface of Mars is therefore crucial to evaluate the food productivity and whether fertilizer supplies from Earth are necessary for sustainable and productive agriculture on Mars. Exploring the composition of modern regolith and eolian deposits with regolith-like compositions such as the Stimson formation and the Greenheugh pediment in Gale crater is the key for future human exploration.

## **5-2.2. Toxicity of Transition Metals for Humans**

Although humans are regularly sent to the International Space Station and astronauts flew back and forth to the Moon during the Apollo era, human health during long-duration missions such as to Mars will remain a significant challenge. In addition to the exposure to radiation, one of the potential threats that will likely impact human exploration is the martian dust that is

omnipresent in the atmosphere and the regolith. As experienced by the *Opportunity* rover that stopped operating in 2018 due to insufficient solar energy during the darkest days of a severe dust storm, dust circulation in the atmosphere is particularly tenacious on Mars, which will likely impact human health, the sustainability of the space suits and habitats, and surface operations (e.g., Harrington et al., 2018). On the Moon, the Apollo missions showed that because fine dust particles were widespread on astronaut space suits, lunar dust was carried into the astronaut's habitat causing them to experience undesired effects, especially on their skin and eyes (Linnarsson et al., 2012). In addition to the small size of particles that can cause health issues such as lung cancer (Cain, 2010), toxic effects of dust are also attributed to the presence of transition metals in the lunar dust, which is considered as a risk for martian exploration, as mentioned in the NASA Engineering and Safety Center (NESC) workshop report: "Mars dust contains heavy metals, which may gain access to the central nervous system via the olfactory pathway" (Winterhalter et al., 2018).

An extensive database (<https://www.atsdr.cdc.gov/substances/indexAZ.asp>) based on the latest research provides an overview of the toxic substances and diseases they can cause. According to this database, each of the metals currently measured by rover instruments at the surface of Mars (Cr, Mn, Co, Ni, Cu, and Zn) can affect organ systems above a certain concentration threshold. Affected systems include the immune, renal, and respiratory systems for Cr, including carcinogenic effects when inhaled, and the digestive, blood, and respiratory systems for Zn. Manganese is known to be hepatotoxic and/or nephrotoxic, Cu is endocrine-disrupting, and Ni can be allergenic (Koller & Saleh, 2018). Above a certain concentration, these metals can thus quickly become a threat for humans when inhaled or ingested, and can ultimately cause death (e.g., Guertin et al., 2004).

To be toxic, transition metals must be in the environment occupied by humans and need to be in a chemical form that is able to enter tissues and cells (Gough et al., 1979). The speciation and redox properties of these metals are thus critical to assessing the toxicity of an element. One potential pathway into cells is substitution, in which metals remove or displace original metals from their binding sites on a cell or cell constituent, such that metals bind with protein site, causing cells to malfunction which, in turn, results in toxicity (Jaishankar et al., 2014). For instance, Cr exists on Earth as five speciation forms from  $\text{Cr}^{2-}$  to  $\text{Cr}^{6+}$ , and the most common and stable species, i.e.,  $\text{Cr}^{3+}$  and  $\text{Cr}^{6+}$ , are toxic. According to terrestrial studies, Cr(VI) is much more dangerous and carcinogenic than Cr(III), partly due to its oxidized form that is highly soluble in water, which enables it to enter cells more readily than the insoluble Cr(III) form (e.g., Nriagu and Nieboer, 1988; Langård, 2013). One of the most serious toxicity effects of



Cr(VI) is as a carcinogen, especially because Cr(VI) is a powerful oxidizing agent. Its reduction within cells by specific reducing agents can lead to the formation of a significant amount of free radicals such as  $\bullet\text{OH}$  when reacting with intracellular  $\text{H}_2\text{O}_2$ . The release of such reactive oxygen radicals eventually causes an oxidative stress that triggers the alteration of the DNA and proteins, i.e., mutations (Shi & Dalal, 1990), leading to carcinogenesis. Depending on the exposure time and on the concentration of Cr(VI), human health can be endangered, and being aware of the amount of such a species in the martian dust is critical for human survival. The toxic level of chromate was determined in the 60's at  $\sim 270$  ppm (Bowen, 1966), and in the 1990s the median lethal dose of  $\text{Cr}^{6+}$  in a compound like  $\text{Na}_2\text{CrO}_4$  was estimated between 50-150 ppm (Katz & Salem, 1993). The total chromium drinking water standard is  $< 0.05$  ppm (WHO report, 2003) and concentrations of Cr(VI) up to 20 ppm in groundwater in India was sufficient to cause gastrointestinal and dermatological issues (Sharma et al., 2012). The average of chromium concentration in martian soils as measured by the *Curiosity* and MER rover is  $\text{Cr} = 2,530\text{-}2,950$  ppm (O'Connell-Cooper et al., 2016), but the amount of  $\text{Cr}^{3+}$  and  $\text{Cr}^{6+}$  is unknown. If toxic amounts of Cr(VI) are contained in martian soils, an excessive exposure could cause health issues, illustrating how crucial it is to know which chromium form is prevalent in the martian dust, and how meticulous astronauts will have to be when returning to the habitat after dust exposure during surface operations.

While Ni, Zn, and Mn concentration ranges are known within martian soils, the composition of Cu, Co, and other transition metals like Pb that could be toxic to humans are not yet constrained. Martian dust is considered to originate from a combination of mechanical erosion and (limited) chemical alteration of parent magmatic rocks, with the current primary dust production rate likely to be derived from reworking of sediments (Bridges & Muhs, 2012; Walter Goetz et al., 2005). A reliable and accurate knowledge of the distribution of transition metals at the surface of Mars is therefore fundamental for the well-being and survival of future astronauts who will explore Mars.

## 6. Conclusion

Transition metal elements usually found in minor and trace amounts in silicate rocks have been observed in elevated concentrations in both martian meteorites and at the surface of Mars. We present the first compilation of all rocks and soils containing such elevated abundances as measured by ChemCam and APXS, the two instruments with chemical composition determination capability onboard the *Curiosity* rover. Such an original compilation emphasizes the remarkable set of transition metals that are anomalously high in Gale crater and highlights

how the fluid history within and in the vicinity of Gale must have been complex. At least one metal deposit of either a hydrothermal or magmatic-hydrothermal type exists in the catchment of Gale crater and is the first metal deposit implied at the surface of Mars. The circulation of groundwater through crater floor sediments likely accumulated transition metals initially contained in their host rock, and precipitated them as sulfides, sulfates, oxides, and silicates within sediments that were later lithified. Diagenetic fluids, sometimes oxidized, precipitated transition metals too within diagenetic features including fractures, veins, and nodules.

The combination of all the following expands the range of metal deposits expected at the surface of Mars: a large variety of magmas from mafic to felsic with high extent of fractional crystallization, the widespread hydrothermal circulation often related to extensive impacts, and the complex fluid history that might be more common than just localized in Gale crater. The Mars 2020 mission will certainly provide evidence for additional environmental settings with abundant transition metals, which will allow us to better constrain the distribution of transition metals on Mars. Such information is essential to assess the potentiality of ancient life on Mars, as transition metals are a necessity for organisms' development and survival, as well as toxic above a certain threshold. Transition metals are key for the perspective of sustainable human missions on Mars due to their role in agriculture and plant growth. Based on experiences with lunar dust during the *Apollo* missions, martian dust can also contain toxic levels of transition metals and estimating an accurate abundance of metals in the regolith and at the surface of Mars is therefore essential for developing successful future man missions.

## 7. Acknowledgments

V.P.'s work was supported by the MSL Participating Scientist Program awards of Mark Salvatore and Christopher Edwards

## 8. Open Research

### Data Availability Statement

ChemCam data presented in the paper are available through Patrick J. Gasda et al. (2021), Johnson et al. (2020), Lanza et al. (2014) and (2016), Lasue et al., (2016) and (2020), Meslin et al. (2019), Nachon et al. (2017), and Payré et al. (2019) publications, and in Table S1. APXS data are publicly available on the Planetary Data System (<https://pds-geosciences.wustl.edu/missions/msl/apxs.htm>) and Table S2.

## 9. References

- Abramov, O., & Kring, D. A. (2005). Impact-induced hydrothermal activity on early Mars. *Journal of Geophysical Research*, 110(E12). <https://doi.org/10.1029/2005JE002453>
- Alloway, B. J. (2013). Heavy Metals and Metalloids as Micronutrients for Plants and Animals. In B. J. Alloway (Ed.), *Heavy Metals in Soils: Trace Metals and Metalloids in Soils and their Bioavailability* (pp. 195–209). Dordrecht: Springer Netherlands. [https://doi.org/10.1007/978-94-007-4470-7\\_7](https://doi.org/10.1007/978-94-007-4470-7_7)
- Allwood, A. C., Wade, L. A., Foote, M. C., Elam, W. T., Hurowitz, J. A., Battel, S., et al. (2020). PIXL: Planetary Instrument for X-Ray Lithochemistry. *Space Science Reviews*, 216(8), 134. <https://doi.org/10.1007/s11214-020-00767-7>
- Ames, D. E., Davidson, A., & Wodicka, N. (2008). Geology of the Giant Sudbury Polymetallic Mining Camp, Ontario, Canada. *Economic Geology*, 103(5), 1057–1077. <https://doi.org/10.2113/gsecongeo.103.5.1057>
- Anderson, R., Bridges, J. C., Williams, A., Edgar, L., Ollila, A., Williams, J., et al. (2015). ChemCam results from the Shaler outcrop in Gale crater, Mars. *Icarus*, 249, 2–21. <https://doi.org/10.1016/j.icarus.2014.07.025>
- Banham, S. G., Gupta, S., Rubin, D. M., Watkins, J. A., Sumner, D. Y., Edgett, K. S., et al. (2018). Ancient Martian aeolian processes and palaeomorphology reconstructed from the Stimson formation on the lower slope of Aeolis Mons, Gale crater, Mars. *Sedimentology*, 65(4), 993–1042. <https://doi.org/10.1111/sed.12469>
- Baumgartner, R. J., Fiorentini, M. L., Lorand, J.-P., Baratoux, D., Zaccarini, F., Ferrière, L., et al. (2017). The role of sulfides in the fractionation of highly siderophile and chalcophile elements during the formation of martian shergottite meteorites. *Geochimica et Cosmochimica Acta*, 210, 1–24. <https://doi.org/10.1016/j.gca.2017.04.011>

822 Beaty, D., Niles, P., Hays, L., Bass, D., Bell, M. S., Bleacher, J., & Rice, M. (2015). *Candidate*  
823 *Scientific Objectives for the Human Exploration of Mars, and Implications for the*  
824 *Identification of Martian Exploration Zones* (MEPAG). Pasadena, CA, United States:  
825 Jet Propulsion Laboratory.

826 Becker, S., Feldmann, J., Wiedemann, S., Okamura, H., Schneider, C., Iwan, K., et al. (2019).  
827 Unified prebiotically plausible synthesis of pyrimidine and purine RNA  
828 ribonucleotides. *Science*, 366(6461), 76–82. <https://doi.org/10.1126/science.aax2747>

829 Berger, J. A., Schmidt, M. E., Gellert, R., Boyd, N. I., Desouza, E. D., Flemming, R. L., et al.  
830 (2017). Zinc and Germanium in the Sedimentary Rocks of Gale Crater on Mars Indicate  
831 Hydrothermal Enrichment Followed by Diagenetic Fractionation. *Journal of*  
832 *Geophysical Research: Planets*. <https://doi.org/10.1002/2017JE005290>

833 Bibring, J.-P., Langevin, Y., Mustard, J. F., Poulet, F., Arvidson, R., Gendrin, A., et al. (2006).  
834 Global Mineralogical and Aqueous Mars History Derived from OMEGA/Mars Express  
835 Data. *Science*, 312(5772), 400–404. <https://doi.org/10.1126/science.1122659>

836 Blake, D., Vaniman, D., Achilles, C., Anderson, R., Bish, D., Bristow, T., et al. (2012).  
837 Characterization and Calibration of the CheMin Mineralogical Instrument on Mars  
838 Science Laboratory. *Space Science Reviews*, 170(1–4), 341–399.  
839 <https://doi.org/10.1007/s11214-012-9905-1>

840 Bowen, H. J. M. (1966). Trace elements in biochemistry. *Trace Elements in Biochemistry*.  
841 Retrieved from <https://www.cabdirect.org/cabdirect/abstract/19671702876>

842 Bridges, N. T., & Muhs, D. R. (2012). Duststones on Mars: Source, Transport, Deposition, and  
843 Erosion. <https://doi.org/10.2110/pec.12.102.0169>

844 Bryk, A. B., Dietrich, W. E., Lamb, M. P., Grotzinger, J. P., Vasavada, A. R., Stack, K. M., et  
845 al. (2019). What was the Original Extent of the Greenheugh Pediment and Gediz Vallis  
846 Ridge Deposits in Gale Crater, Mars? *LPI Contributions*, 2089, 6296.

847 Bubenheim, D. L., Bates, M. E., & Flynn, M. T. (1995). *An Approach for Development of*  
848 *Regenerative Life Support Systems for Human Habitats in Space* (SAE Technical Paper  
849 No. 951730). Warrendale, PA: SAE International. <https://doi.org/10.4271/951730>

850 Cain, J. R. (2010). Lunar dust: The Hazard and Astronaut Exposure Risks. *Earth Moon and*  
851 *Planets*, 107(1), 107–125. <https://doi.org/10.1007/s11038-010-9365-0>

852 Carr, M. H., & Head, J. W. (2015). Martian surface/near-surface water inventory: Sources,  
853 sinks, and changes with time. *Geophysical Research Letters*, 42(3), 726–732.  
854 <https://doi.org/10.1002/2014GL062464>

855 Clark, B. C., Kolb, V. M., Steele, A., House, C. H., Lanza, N. L., Gasda, P. J., et al. (2021).  
856 Origin of Life on Mars: Suitability and Opportunities. *Life*, 11(6), 539.  
857 <https://doi.org/10.3390/life11060539>

858 Cockell, C. s., Bush, T., Bryce, C., Direito, S., Fox-Powell, M., Harrison, J. p., et al. (2016).  
859 Habitability: A Review. *Astrobiology*, 16(1), 89–117.  
860 <https://doi.org/10.1089/ast.2015.1295>

861 Cotton, C. A., Edlich-Muth, C., & Bar-Even, A. (2018). Reinforcing carbon fixation: CO2  
862 reduction replacing and supporting carboxylation. *Current Opinion in Biotechnology*,  
863 49, 49–56. <https://doi.org/10.1016/j.copbio.2017.07.014>

864 Cousin, A., Forni, O., Maurice, S., Gasnault, O., Fabre, C., Sautter, V., et al. (2011). Laser  
865 induced breakdown spectroscopy library for the Martian environment. *Spectrochimica*  
866 *Acta Part B: Atomic Spectroscopy*, 66(11–12), 805–814.  
867 <https://doi.org/10.1016/j.sab.2011.10.004>

868 Cousin, Agnes, Sautter, V., Payré, V., Forni, O., Mangold, N., Gasnault, O., et al. (2017).  
869 Classification of igneous rocks analyzed by ChemCam at Gale crater, Mars. *Icarus*, 288,  
870 265–283. <https://doi.org/10.1016/j.icarus.2017.01.014>

871 Cox, D. P., Lindsey, D. A., Singer, D. A., Moring, B. C., & Diggles, M. F. (2003). Sediment-  
872 Hosted Copper Deposits of the World: Deposit Models and Database. *U.S. Geological*  
873 *Survey Open-File Report*, (03–107). Retrieved from  
874 <http://citeseerx.ist.psu.edu/viewdoc/summary?doi=10.1.1.400.4225>

875 Della Puppa, L., Komárek, M., Bordas, F., Bollinger, J.-C., & Joussein, E. (2013). Adsorption  
876 of copper, cadmium, lead and zinc onto a synthetic manganese oxide. *Journal of Colloid*  
877 *and Interface Science*, 399, 99–106. <https://doi.org/10.1016/j.jcis.2013.02.029>

878 Ehlmann, B. L., & Mustard, J. F. (2012). An in-situ record of major environmental transitions  
879 on early Mars at Northeast Syrtis Major. *Geophysical Research Letters*, 39(11).  
880 <https://doi.org/10.1029/2012GL051594>

881 Ehlmann, B. L., Mustard, J. F., Murchie, S. L., Bibring, J.-P., Meunier, A., Fraeman, A. A., &  
882 Langevin, Y. (2011). Subsurface water and clay mineral formation during the early  
883 history of Mars. *Nature*, 479(7371), 53–60. <https://doi.org/10.1038/nature10582>

884 Eichler, A., Hadland, N., Pickett, D., Masaitis, D., Handy, D., Perez, A., et al. (2021).  
885 Challenging the agricultural viability of Martian regolith simulants. *Icarus*, 354,  
886 114022. <https://doi.org/10.1016/j.icarus.2020.114022>

887 Farrow, C. E. G., & Watkinson, D. H. (1992). Alteration and the role of fluids in Ni, Cu and  
888 platinum-group element deposition, Sudbury Igneous Complex contact, Onaping-  
889 Levack area, Ontario. *Mineralogy and Petrology*, 46(1), 67–83.  
890 <https://doi.org/10.1007/BF01160703>

891 Fischer, W. W., Hemp, J., & Johnson, J. E. (2015). Manganese and the Evolution of  
892 Photosynthesis. *Origins of Life and Evolution of Biospheres*, 45(3), 351–357.  
893 <https://doi.org/10.1007/s11084-015-9442-5>

894 Foley, C. N., Economou, T., & Clayton, R. N. (2003). Final chemical results from the Mars  
895 Pathfinder alpha proton X-ray spectrometer: ALPHA PROTON X-RAY

896 SPECTROMETER RESULTS. *Journal of Geophysical Research: Planets*, 108(E12).  
897 <https://doi.org/10.1029/2002JE002019>

898 Forni, O., Gaft, M., Toplis, M. J., Clegg, S. M., Maurice, S., Wiens, R. C., et al. (2015). First  
899 detection of fluorine on Mars: Implications for Gale Crater's geochemistry: First  
900 detection of fluorine on Mars. *Geophysical Research Letters*, 42(4), 1020–1028.  
901 <https://doi.org/10.1002/2014GL062742>

902 Fox, V. K., Arvidson, R. E., Jolliff, B. L., Carpenter, P. K., Catalano, J. G., Hinkle, M. A. G.,  
903 & Morris, R. V. (2015). Characterization of Synthetic and Natural Manganese Oxides  
904 as Martian Analogues (Vol. 46, p. 2132). Presented at the Lunar and Planetary Science  
905 Conference. Retrieved from <http://adsabs.harvard.edu/abs/2015LPI....46.2132F>

906 Fox, V. K., Bennett, K. A., Bryk, A., Arvidson, R. E., Bristow, T., Dehouck, E., et al. (2020).  
907 One Year in Glen Torridon: Key Results from the Mars Science Laboratory Curiosity  
908 Rover Exploration of Clay-Bearing Units, 51, 2833. Presented at the Lunar and  
909 Planetary Science Conference.

910 Fraeman, A. A., Edgar, L. A., Rampe, E. B., Thompson, L. M., Frydenvang, J., Fedo, C. M., et  
911 al. (2020). Evidence for a Diagenetic Origin of Vera Rubin Ridge, Gale Crater, Mars:  
912 Summary and Synthesis of Curiosity's Exploration Campaign. *Journal of Geophysical*  
913 *Research: Planets*, 125(12), e2020JE006527. <https://doi.org/10.1029/2020JE006527>

914 Frydenvang, J., Mangold, N., Wiens, R. C., Fraeman, A. A., Edgar, L. A., Fedo, C. M., et al.  
915 (2020). The Chemostratigraphy of the Murray Formation and Role of Diagenesis at  
916 Vera Rubin Ridge in Gale Crater, Mars, as Observed by the ChemCam Instrument.  
917 *Journal of Geophysical Research: Planets*, 125(9), e2019JE006320.  
918 <https://doi.org/10.1029/2019JE006320>

919 Gadd, G. M. (1992). Metals and microorganisms: A problem of definition. *FEMS Microbiology*  
920 *Letters*, 100(1), 197–203. [https://doi.org/10.1016/0378-1097\(92\)90209-7](https://doi.org/10.1016/0378-1097(92)90209-7)

921 Gaillard, F., & Scaillet, B. (2009). The sulfur content of volcanic gases on Mars. *Earth and*  
922 *Planetary Science Letters*, 279(1), 34–43. <https://doi.org/10.1016/j.epsl.2008.12.028>

923 Gasda, P. J., Lanza, N., Meslin, P.-Y., Forni, O., L’Haridon, J., Fischer, W. W., et al. (2019a).  
924 High-Mn Sandstone as Evidence for Oxidized Conditions in Gale Crater Lake (Vol. 50,  
925 p. 1620). Presented at the LPSC. Retrieved from  
926 <http://adsabs.harvard.edu/abs/2019LPI....50.1620G>

927 Gasda, P. J., Lanza, N., Meslin, P.-Y., Forni, O., L’Haridon, J., Fischer, W. W., et al. (2019b).  
928 High-Mn Sandstone as Evidence for Oxidized Conditions in Gale Crater Lake (Vol. 50,  
929 p. 1620). Presented at the LPSC. Retrieved from  
930 <http://adsabs.harvard.edu/abs/2019LPI....50.1620G>

931 Gasda, Patrick J., Anderson, R. B., Cousin, A., Forni, O., Clegg, S. M., Ollila, A., et al. (2021).  
932 Quantification of manganese for ChemCam Mars and laboratory spectra using a  
933 multivariate model. *Spectrochimica Acta Part B: Atomic Spectroscopy*, 181, 106223.  
934 <https://doi.org/10.1016/j.sab.2021.106223>

935 Gellert, R., Clark, B. C., & MSL and MER Science Teams. (2015). In Situ Compositional  
936 Measurements of Rocks and Soils with the Alpha Particle X-ray Spectrometer on  
937 NASA’s Mars Rovers. *Elements*, 11(1), 39–44.  
938 <https://doi.org/10.2113/gselements.11.1.39>

939 Goetz, W., Wiens, R. C., Dehouck, E., Gasnault, O., Lasue, J., Payre, V., et al. (2020a).  
940 Tracking of Copper by the ChemCam Instrument in Gale Crater, Mars: Elevated  
941 Abundances in Glen Torridon, 51, 2974. Presented at the Lunar and Planetary Science  
942 Conference.

943 Goetz, W., Wiens, R. C., Dehouck, E., Gasnault, O., Lasue, J., Payre, V., et al. (2020b).  
944 Tracking of Copper by the ChemCam Instrument in Gale Crater, Mars: Elevated



945 Abundances in Glen Torridon, 51, 2974. Presented at the Lunar and Planetary Science  
 946 Conference.

947 Goetz, Walter, Bertelsen, P., Binau, C. S., Gunnlaugsson, H. P., Hviid, S. F., Kinch, K. M., et  
 948 al. (2005). Indication of drier periods on Mars from the chemistry and mineralogy of  
 949 atmospheric dust. *Nature*, 436(7047), 62–65. <https://doi.org/10.1038/nature03807>

950 Goudge, T. A., Mustard, J. F., Head, J. W., Fassett, C. I., & Wiseman, S. M. (2015). Assessing  
 951 the mineralogy of the watershed and fan deposits of the Jezero crater paleolake system,  
 952 Mars. *Journal of Geophysical Research: Planets*, 120(4), 775–808.  
 953 <https://doi.org/10.1002/2014JE004782>

954 Gough, L. P., Shacklette, H. T., Case, A. A., & Survey (U.S.), G. (1979). *Element*  
 955 *Concentrations Toxic to Plants, Animals, and Man: An Appraisal of the Toxicity Hazard*  
 956 *to Plants, Animals, and Man from Natural and Manmade Element Concentrations of*  
 957 *Environmental Concern*. U.S. Department of the Interior, Geological Survey.

958 Grotzinger, J. P., Gupta, S., Malin, M. C., Rubin, D. M., Schieber, J., Siebach, K., et al. (2015a).  
 959 Deposition, exhumation, and paleoclimate of an ancient lake deposit, Gale crater, Mars.  
 960 *Science*, 350(6257), aac7575–aac7575. <https://doi.org/10.1126/science.aac7575>

961 Grotzinger, J. P., Gupta, S., Malin, M. C., Rubin, D. M., Schieber, J., Siebach, K., et al. (2015b).  
 962 Deposition, exhumation, and paleoclimate of an ancient lake deposit, Gale crater, Mars.  
 963 *Science*, 350(6257), aac7575–aac7575. <https://doi.org/10.1126/science.aac7575>

964 Grotzinger, John P., Crisp, J., Vasavada, A. R., Anderson, R. C., Baker, C. J., Barry, R., et al.  
 965 (2012). Mars Science Laboratory Mission and Science Investigation. *Space Science*  
 966 *Reviews*, 170(1–4), 5–56. <https://doi.org/10.1007/s11214-012-9892-2>

967 Guertin, J., Jacobs, J. A., & Avakian, C. P. (2004). *Chromium(VI) Handbook*. CRC Press.

968 Hardgrove, C., Johnson, J., Rice, M., Bell, J., Kinch, K., Wellington, D., et al. (2015). Detecting  
 969 High Manganese Phases in Curiosity Mastcam Multispectral Images and Chemcam

970 Passive Visible to Near Infrared Spectra (Vol. 46, p. 2748). Presented at the Lunar and  
 971 Planetary Science Conference. Retrieved from  
 972 <http://adsabs.harvard.edu/abs/2015LPI....46.2748H>

973 Harrington, A. D., Zeigler, R. A., & McCubbin, F. M. (2018). The Need for Medical Geology  
 974 in Space Exploration: Implications for the Journey to Mars and Beyond. Presented at  
 975 the Lunar and Planetary Science Conference, The Woodlands, TX, United States.

976 Hitzman, M. W., Reynolds, N. A., Sangster, D. F., Allen, C. R., & Carman, C. E. (2003).  
 977 Classification, Genesis, and Exploration Guides for Nonsulfide Zinc Deposits.  
 978 *Economic Geology*, 98(4), 685–714. <https://doi.org/10.2113/gsecongeo.98.4.685>

979 Hoppert, M. (2011). Metalloenzymes. In J. Reitner & V. Thiel (Eds.), *Encyclopedia of*  
 980 *Geobiology* (pp. 558–563). Dordrecht: Springer Netherlands.  
 981 [https://doi.org/10.1007/978-1-4020-9212-1\\_134](https://doi.org/10.1007/978-1-4020-9212-1_134)

982 Horgan, B. H. N., Anderson, R. B., Dromart, G., Amador, E. S., & Rice, M. S. (2020). The  
 983 mineral diversity of Jezero crater: Evidence for possible lacustrine carbonates on Mars.  
 984 *Icarus*, 339, 113526. <https://doi.org/10.1016/j.icarus.2019.113526>

985 Hughes, M. N., & Poole, R. (1989). *Metals and Microorganisms*. Springer Netherlands.  
 986 Retrieved from <https://www.springer.com/gp/book/9780412244001>

987 Humayun, M., Nemchin, A., Zanda, B., Hewins, R. H., Grange, M., Kennedy, A., et al. (2013).  
 988 Origin and age of the earliest Martian crust from meteorite NWA 7533. *Nature*,  
 989 503(7477), 513–516. <https://doi.org/10.1038/nature12764>

990 Hurowitz, J. A., Grotzinger, J. P., Fischer, W. W., McLennan, S. M., Milliken, R. E., Stein, N.,  
 991 et al. (2017). Redox stratification of an ancient lake in Gale crater, Mars. *Science*,  
 992 356(6341), eaah6849. <https://doi.org/10.1126/science.aah6849>

993 Jaishankar, M., Tseten, T., Anbalagan, N., Mathew, B. B., & Beeregowda, K. N. (2014).  
 994 Toxicity, mechanism and health effects of some heavy metals. *Interdisciplinary*  
 995 *Toxicology*, 7(2), 60–72. <https://doi.org/10.2478/intox-2014-0009>  
 996 Johnson, J. R., Meslin, P. Y., Bell, J. F., Wiens, R. C., Maurice, S., Gasnault, O., & Rapin, W.  
 997 (2020a). Progress on Iron Meteorite Detections by the Mars Science Laboratory  
 998 Curiosity Rover, 51, 1136. Presented at the Lunar and Planetary Science Conference.  
 999 Johnson, J. R., Meslin, P. Y., Bell, J. F., Wiens, R. C., Maurice, S., Gasnault, O., & Rapin, W.  
 1000 (2020b). Progress on Iron Meteorite Detections by the Mars Science Laboratory  
 1001 Curiosity Rover, 51, 1136. Presented at the Lunar and Planetary Science Conference.  
 1002 Johnson, J. R., Bell, J. F., Wiens, R. C., Maurice, S., Gasnault, O., Jacob, S., & Dietrich, W. E.  
 1003 (2021a). New Iron Meteorite Detections by the Mars Science Laboratory Curiosity  
 1004 Rover in the Southern Glen Torridon Region, 1212. Presented at the Lunar and  
 1005 Planetary Science Conference.  
 1006 Johnson, J. R., Bell, J. F., Wiens, R. C., Maurice, S., Gasnault, O., Jacob, S., & Dietrich, W. E.  
 1007 (2021b). New Iron Meteorite Detections by the Mars Science Laboratory Curiosity  
 1008 Rover in the Southern Glen Torridon Region, 1212. Presented at the Lunar and  
 1009 Planetary Science Conference.  
 1010 Katz, S. A., & Salem, H. (1993). The toxicology of chromium with respect to its chemical  
 1011 speciation: A review. *Journal of Applied Toxicology*, 13(3), 217–224.  
 1012 <https://doi.org/10.1002/jat.2550130314>  
 1013 King, P. L., & McLennan, S. M. (2010). Sulfur on Mars. *Elements*, 6(2), 107–112.  
 1014 <https://doi.org/10.2113/gselements.6.2.107>  
 1015 King, P. L., & McSween, H. Y. (2005). Effects of H<sub>2</sub>O, pH, and oxidation state on the stability  
 1016 of Fe minerals on Mars. *Journal of Geophysical Research: Planets*, 110(E12).  
 1017 <https://doi.org/10.1029/2005JE002482>

1018 Knoll, A. H., & Grotzinger, J. (2006). Water on Mars and the Prospect of Martian Life.  
 1019 *Elements*, 2(3), 169–173. <https://doi.org/10.2113/gselements.2.3.169>

1020 Koller, M., & Saleh, H. M. (2018). Introductory Chapter: Introducing Heavy Metals. *Heavy*  
 1021 *Metals*. <https://doi.org/10.5772/intechopen.74783>

1022 Langård, S. (2013). *Biological and Environmental Aspects of Chromium*. Elsevier.

1023 Lanza, N. L., Fischer, W. W., Wiens, R. C., Grotzinger, J., Ollila, A. M., Cousin, A., et al.  
 1024 (2014). High manganese concentrations in rocks at Gale crater, Mars. *Geophysical*  
 1025 *Research Letters*, 41(16), 5755–5763. <https://doi.org/10.1002/2014GL060329>

1026 Lanza, N. L., Wiens, R. C., Arvidson, R. E., Clark, B. C., Fischer, W. W., Gellert, R., et al.  
 1027 (2016a). Oxidation of manganese in an ancient aquifer, Kimberley formation, Gale  
 1028 crater, Mars: Manganese Fracture Fills in Gale Crater. *Geophysical Research Letters*,  
 1029 43(14), 7398–7407. <https://doi.org/10.1002/2016GL069109>

1030 Lanza, N. L., Wiens, R. C., Arvidson, R. E., Clark, B. C., Fischer, W. W., Gellert, R., et al.  
 1031 (2016b). Oxidation of manganese in an ancient aquifer, Kimberley formation, Gale  
 1032 crater, Mars: Manganese Fracture Fills in Gale Crater. *Geophysical Research Letters*,  
 1033 43(14), 7398–7407. <https://doi.org/10.1002/2016GL069109>

1034 Lapen, T. J., Richter, M., Brandon, A. D., Debaille, V., Beard, B. L., Shafer, J. T., & Peslier,  
 1035 A. H. (2010). A Younger Age for ALH84001 and Its Geochemical Link to Shergottite  
 1036 Sources in Mars. *Science*, 328(5976), 347–351.  
 1037 <https://doi.org/10.1126/science.1185395>

1038 Lapotre, M. G. A., Lamb, M. P., & Williams, R. M. E. (2016). Canyon formation constraints  
 1039 on the discharge of catastrophic outburst floods of Earth and Mars. *Journal of*  
 1040 *Geophysical Research: Planets*, 121(7), 1232–1263.  
 1041 <https://doi.org/10.1002/2016JE005061>

1042 Lasue, J., Clegg, S. M., Forni, O., Cousin, A., Wiens, R. C., Lanza, N., et al. (2016a).  
 1043 Observation of > 5 wt % zinc at the Kimberley outcrop, Gale crater, Mars. *Journal of*  
 1044 *Geophysical Research: Planets*, 121(3), 2015JE004946.  
 1045 <https://doi.org/10.1002/2015JE004946>  
 1046 Lasue, J., Clegg, S. M., Forni, O., Cousin, A., Wiens, R. C., Lanza, N., et al. (2016b).  
 1047 Observation of > 5 wt % zinc at the Kimberley outcrop, Gale crater, Mars. *Journal of*  
 1048 *Geophysical Research: Planets*, 121(3), 2015JE004946.  
 1049 <https://doi.org/10.1002/2015JE004946>  
 1050 Lasue, J., Meslin, P. Y., Sautter, V., Maroger, I., Krämer Ruggiu, L., Bridges, J. C., et al. (2019).  
 1051 Probable Chondritic Fragments Detected by ChemCam in Gale Crater. In *Lunar and*  
 1052 *Planetary Science Conference*. The Woodlands, United States. Retrieved from  
 1053 <https://hal.archives-ouvertes.fr/hal-02411470>  
 1054 Lasue, J., Meslin, P.-Y., Cohen, B. A., Sautter, V., Bridges, J. C., Lewin, E., et al. (2020).  
 1055 Gretna Green, a Possible Chondrite Detected at Glen Torridon in Gale Crater, 2125.  
 1056 Presented at the Lunar and Planetary Science Conference.  
 1057 Le Deit, L., Mangold, N., Forni, O., Cousin, A., Lasue, J., Schröder, S., et al. (2016). The  
 1058 potassic sedimentary rocks in Gale Crater, Mars, as seen by ChemCam on board  
 1059 Curiosity. *Journal of Geophysical Research: Planets*, 121(5), 2015JE004987.  
 1060 <https://doi.org/10.1002/2015JE004987>  
 1061 Le Deit, Laetitia, Hauber, E., Fueten, F., Pondrelli, M., Rossi, A. P., & Jaumann, R. (2013).  
 1062 Sequence of infilling events in Gale Crater, Mars: Results from morphology,  
 1063 stratigraphy, and mineralogy. *Journal of Geophysical Research: Planets*, 118(12),  
 1064 2439–2473. <https://doi.org/10.1002/2012JE004322>  
 1065 L’Haridon, J., Mangold, N., Fraeman, A. A., Johnson, J. R., Cousin, A., Rapin, W., et al. (2020).  
 1066 Iron Mobility During Diagenesis at Vera Rubin Ridge, Gale Crater, Mars. *Journal of*

1067 *Geophysical Research: Planets*, 125(11), e2019JE006299.  
 1068 <https://doi.org/10.1029/2019JE006299>  
 1069 Lingappa, U. F., Monteverde, D. R., Magyar, J. S., Valentine, J. S., & Fischer, W. W. (2019).  
 1070 How manganese empowered life with dioxygen (and vice versa). *Free Radical Biology*  
 1071 *and Medicine*, 140, 113–125. <https://doi.org/10.1016/j.freeradbiomed.2019.01.036>  
 1072 Linnarsson, D., Carpenter, J., Fubini, B., Gerde, P., Karlsson, L. L., & Loftus, D. J. (2012).  
 1073 Toxicity of lunar dust. *Planetary and Space Science*, 74(1), 57–71.  
 1074 Lorand, J. -P., Hewins, R. H., Humayun, M., Remusat, L., Zanda, B., La, C., & Pont, S. (2018).  
 1075 Chalcophile-siderophile element systematics of hydrothermal pyrite from martian  
 1076 regolith breccia NWA 7533. *Geochimica et Cosmochimica Acta*, 241, 134–149.  
 1077 <https://doi.org/10.1016/j.gca.2018.08.041>  
 1078 Lorand, Jean-Pierre, Chevrier, V., & Sautter, V. (2005). Sulfide mineralogy and redox  
 1079 conditions in some shergottites. *Meteoritics & Planetary Science*, 40(8), 1257–1272.  
 1080 <https://doi.org/10.1111/j.1945-5100.2005.tb00187.x>  
 1081 Lorand, Jean-Pierre, Hewins, R. H., Remusat, L., Zanda, B., Pont, S., Leroux, H., et al. (2015).  
 1082 Nickeliferous pyrite tracks pervasive hydrothermal alteration in Martian regolith  
 1083 breccia: A study in NWA 7533. *Meteoritics & Planetary Science*, 50(12), 2099–2120.  
 1084 <https://doi.org/10.1111/maps.12565>  
 1085 Marschner, P. (1995). *Mineral Nutrition of Higher Plants*. London, UK: Academic Press.  
 1086 <https://doi.org/10.1016/C2009-0-63043-9>  
 1087 Maurice, S., Wiens, R. C., Saccoccio, M., Barraclough, B., Gasnault, O., Forni, O., et al. (2012).  
 1088 The ChemCam Instrument Suite on the Mars Science Laboratory (MSL) Rover: Science  
 1089 Objectives and Mast Unit Description. *Space Science Reviews*, 170(1–4), 95–166.  
 1090 <https://doi.org/10.1007/s11214-012-9912-2>

1091 Maurice, S., Wiens, R. C., Bernardi, P., & Cais, P. (2021). The SuperCam instrument suite on  
 1092 the Mars 2020 rover: Science objectives and mast-unit description. *Space Science*  
 1093 *Reviews*, 217(SPAC-D-20-00069R1).

1094 McCubbin, F. M., Boyce, J. W., Novak-Szabo, T., Santos, A., Tartese, R., Muttik, N., et al.  
 1095 (2016). Geologic history of Martian regolith breccia Northwest Africa 7034: Evidence  
 1096 for hydrothermal activity and lithologic diversity in the Martian crust. *Journal of*  
 1097 *Geophysical Research E: Planets*, 121(10), 21202149.  
 1098 <https://doi.org/10.1002/2016JE005143>

1099 McCubbin, F. M., Boyce, J. W., Srinivasan, P., Santos, A. R., Elardo, S. M., Filiberto, J., et al.  
 1100 (2016). Heterogeneous distribution of H<sub>2</sub>O in the Martian interior: Implications for the  
 1101 abundance of H<sub>2</sub>O in depleted and enriched mantle sources. *Meteoritics & Planetary*  
 1102 *Science*, 51(11), 2036–2060. <https://doi.org/10.1111/maps.12639>

1103 McLennan, S. M., Anderson, R. B., Bell, J. F., Bridges, J. C., Calef, F., Campbell, J. L., et al.  
 1104 (2014). Elemental Geochemistry of Sedimentary Rocks at Yellowknife Bay, Gale  
 1105 Crater, Mars. *Science*, 343(6169), 1244734–1244734.  
 1106 <https://doi.org/10.1126/science.1244734>

1107 McSween, H. Y., Murchie, S. L., Crisp, J. A., Bridges, N. T., Anderson, R. C., Bell, J. F., et al.  
 1108 (1999). Chemical, multispectral, and textural constraints on the composition and origin  
 1109 of rocks at the Mars Pathfinder landing site. *Journal of Geophysical Research: Planets*,  
 1110 104(E4), 8679–8715. <https://doi.org/10.1029/98JE02551>

1111 McSween, H. Y., Ruff, S. W., Morris, R. V., Bell, J. F., Herkenhoff, K., Gellert, R., et al.  
 1112 (2006). Alkaline volcanic rocks from the Columbia Hills, Gusev crater, Mars. *Journal*  
 1113 *of Geophysical Research*, 111(E9). <https://doi.org/10.1029/2006JE002698>

1114 Meslin, P.-Y., Gasda, P., L'Haridon, J., Forni, O., Lanza, N., Lamm, S., et al. (2018). Detection  
 1115 of Hydrous Manganese and Iron Oxides with Variable Phosphorus and Magnesium

1116 Contents in the Lacustrine Sediments of the Murray Formation, Gale, Mars, *49*, 1447.  
1117 Presented at the Lunar and Planetary Science Conference.

1118 Meslin, P.-Y., Wellington, D., Wiens, R. C., Johnson, J. R., Van Beek, J., Gasnault, O., et al.  
1119 (2019a). Diversity and Areal Density of Iron-Nickel Meteorites Analyzed by Chemcam  
1120 in Gale Crater, *50*, 3179. Presented at the Lunar and Planetary Science Conference.

1121 Meslin, P.-Y., Wellington, D., Wiens, R. C., Johnson, J. R., Van Beek, J., Gasnault, O., et al.  
1122 (2019b). Diversity and Areal Density of Iron-Nickel Meteorites Analyzed by Chemcam  
1123 in Gale Crater, *50*, 3179. Presented at the Lunar and Planetary Science Conference.

1124 Michalski, J. R., Dobreá, E. Z. N., Niles, P. B., & Cuadros, J. (2017). Ancient hydrothermal  
1125 seafloor deposits in Eridania basin on Mars. *Nature Communications*, *8*(1), 15978.  
1126 <https://doi.org/10.1038/ncomms15978>

1127 Milliken, R. E., Grotzinger, J. P., & Thomson, B. J. (2010). Paleoclimate of Mars as captured  
1128 by the stratigraphic record in Gale Crater: STRATIGRAPHY OF GALE CRATER.  
1129 *Geophysical Research Letters*, *37*(4). <https://doi.org/10.1029/2009GL041870>

1130 Ming, D. W., Gellert, R., Morris, R. V., Arvidson, R. E., Brückner, J., Clark, B. C., et al. (2008).  
1131 Geochemical properties of rocks and soils in Gusev Crater, Mars: Results of the Alpha  
1132 Particle X-Ray Spectrometer from Cumberland Ridge to Home Plate. *Journal of*  
1133 *Geophysical Research*, *113*(E12). <https://doi.org/10.1029/2008JE003195>

1134 Morris, R. V., Rampe, E. B., Vaniman, D. T., Christoffersen, R., Yen, A. S., Morrison, S. M.,  
1135 et al. (2020). Hydrothermal Precipitation of Sanidine (Adularia) Having Full Al,Si  
1136 Structural Disorder and Specular Hematite at Maunakea Volcano (Hawai'i) and at Gale  
1137 Crater (Mars). *Journal of Geophysical Research: Planets*, *125*(9), e2019JE006324.  
1138 <https://doi.org/10.1029/2019JE006324>

1139 Nachon, M., Clegg, S. M., Mangold, N., Schröder, S., Kah, L. C., Dromart, G., et al. (2014).  
1140 Calcium sulfate veins characterized by ChemCam/Curiosity at Gale crater, Mars.



1141 *Journal of Geophysical Research: Planets*, 119(9), 1991–2016.  
 1142 <https://doi.org/10.1002/2013JE004588>

1143 Nachon, M., Mangold, N., Forni, O., Kah, L. C., Cousin, A., Wiens, R. C., et al. (2017a).  
 1144 Chemistry of diagenetic features analyzed by ChemCam at Pahrump Hills, Gale crater,  
 1145 Mars. *Icarus*, 281, 121–136. <https://doi.org/10.1016/j.icarus.2016.08.026>

1146 Nachon, M., Mangold, N., Forni, O., Kah, L. C., Cousin, A., Wiens, R. C., et al. (2017b).  
 1147 Chemistry of diagenetic features analyzed by ChemCam at Pahrump Hills, Gale crater,  
 1148 Mars. *Icarus*, 281, 121–136. <https://doi.org/10.1016/j.icarus.2016.08.026>

1149 Nriagu, J. O., & Nieboer, E. (1988). *Chromium in the Natural and Human Environments*. John  
 1150 Wiley & Sons.

1151 O’Connell-Cooper, C. D., Spray, J. G., Thompson, L. M., Gellert, R., Berger, J. A., Boyd, N.  
 1152 I., et al. (2016). APXS-derived chemistry of the Bagnold dune sands: Comparisons with  
 1153 Gale Crater soils and the global Martian average. *Journal of Geophysical Research:*  
 1154 *Planets*, 2623–2643. [https://doi.org/10.1002/2017JE005268@10.1002/\(ISSN\)2169-](https://doi.org/10.1002/2017JE005268@10.1002/(ISSN)2169-9100.DUNE16)  
 1155 9100.DUNE16

1156 O’Connell-Cooper, C. D., Thompson, L. M., Gellert, R., Spray, J. G., Berger, J. A., Boyd, N.  
 1157 I., et al. (2020). APXS Analysis of the Jura and Knockfarril Hill Members of the Murray  
 1158 Formation Within the Glen Torridon Locale, Gale Crater, Mars, 51, 2948. Presented at  
 1159 the Lunar and Planetary Science Conference.

1160 Payré, V., Siebach, K. L., Dasgupta, R., Udry, A., Rampe, E. B., & Morrison, S. M. (2020).  
 1161 Constraining Ancient Magmatic Evolution on Mars Using Crystal Chemistry of Detrital  
 1162 Igneous Minerals in the Sedimentary Bradbury Group, Gale Crater, Mars. *Journal of*  
 1163 *Geophysical Research: Planets*, 125(8), e2020JE006467.  
 1164 <https://doi.org/10.1029/2020JE006467>

1165 Payré, Valérie, Fabre, C., Sautter, V., Cousin, A., Mangold, N., Deit, L. L., et al. (2019a).  
 1166 Copper enrichments in the Kimberley formation in Gale crater, Mars: Evidence for a  
 1167 Cu deposit at the source. *Icarus*, 321, 736–751.  
 1168 <https://doi.org/10.1016/j.icarus.2018.12.015>

1169 Payré, Valérie, Fabre, C., Sautter, V., Cousin, A., Mangold, N., Deit, L. L., et al. (2019b).  
 1170 Copper enrichments in the Kimberley formation in Gale crater, Mars: Evidence for a  
 1171 Cu deposit at the source. *Icarus*, 321, 736–751.  
 1172 <https://doi.org/10.1016/j.icarus.2018.12.015>

1173 Pittman, J. K. (2005). Managing the manganese: molecular mechanisms of manganese transport  
 1174 and homeostasis. *New Phytologist*, 167(3), 733–742. [https://doi.org/10.1111/j.1469-](https://doi.org/10.1111/j.1469-8137.2005.01453.x)  
 1175 [8137.2005.01453.x](https://doi.org/10.1111/j.1469-8137.2005.01453.x)

1176 Ragsdale, S. W. (1991). Enzymology of the Acetyl-CoA Pathway of CO<sub>2</sub> Fixation. *Critical*  
 1177 *Reviews in Biochemistry and Molecular Biology*, 26(3–4), 261–300.  
 1178 <https://doi.org/10.3109/10409239109114070>

1179 Rampe, E. B., Blake, D. F., Bristow, T. F., Ming, D. W., Vaniman, D. T., Morris, R. V., et al.  
 1180 (2020). Mineralogy and geochemistry of sedimentary rocks and eolian sediments in  
 1181 Gale crater, Mars: A review after six Earth years of exploration with Curiosity.  
 1182 *Geochemistry*, 80(2), 125605. <https://doi.org/10.1016/j.chemer.2020.125605>

1183 Rapin, W., Ehlmann, B. L., Dromart, G., Schieber, J., Thomas, N. H., Fischer, W. W., et al.  
 1184 (2019). An interval of high salinity in ancient Gale crater lake on Mars. *Nature*  
 1185 *Geoscience*, 12(11), 889–895. <https://doi.org/10.1038/s41561-019-0458-8>

1186 Richards, J. P. (2009). Postsubduction porphyry Cu-Au and epithermal Au deposits: Products  
 1187 of remelting of subduction-modified lithosphere. *Geology*, 37(3), 247–250.  
 1188 <https://doi.org/10.1130/G25451A.1>

1189 Ridley, J. (2013). *Ore Deposit Geology*. Cambridge: Cambridge University Press.  
1190 <https://doi.org/10.1017/CBO9781139135528>

1191 Ruff, S. W., & Farmer, J. D. (2016). Silica deposits on Mars with features resembling hot spring  
1192 biosignatures at El Tatio in Chile. *Nature Communications*, 7(1), 13554.  
1193 <https://doi.org/10.1038/ncomms13554>

1194 Santos, A. R., Agee, C. B., McCubbin, F. M., Shearer, C. K., Burger, P. V., Tartèse, R., &  
1195 Anand, M. (2015). Petrology of igneous clasts in Northwest Africa 7034: Implications  
1196 for the petrologic diversity of the martian crust. *Geochimica et Cosmochimica Acta*,  
1197 157, 56–85. <https://doi.org/10.1016/j.gca.2015.02.023>

1198 Santos, E. F., Kondo Santini, J. M., Paixão, A. P., Júnior, E. F., Lavres, J., Campos, M., & Reis,  
1199 A. R. dos. (2017). Physiological highlights of manganese toxicity symptoms in soybean  
1200 plants: Mn toxicity responses. *Plant Physiology and Biochemistry*, 113, 6–19.  
1201 <https://doi.org/10.1016/j.plaphy.2017.01.022>

1202 Sautter, V., Toplis, M. J., Wiens, R. C., Cousin, A., Fabre, C., Gasnault, O., et al. (2015). In  
1203 situ evidence for continental crust on early Mars. *Nature Geoscience*, 8(8), 605–609.  
1204 <https://doi.org/10.1038/ngeo2474>

1205 Schwenzer, S. P., Abramov, O., Allen, C. C., Bridges, J. C., Clifford, S. M., Filiberto, J., et al.  
1206 (2012). Gale Crater: Formation and post-impact hydrous environments. *Planetary and*  
1207 *Space Science*, 70(1), 84–95. <https://doi.org/10.1016/j.pss.2012.05.014>

1208 Sharma, P., Bihari, V., Agarwal, S. K., Verma, V., Kesavachandran, C. N., Pangtey, B. S., et  
1209 al. (2012). Groundwater Contaminated with Hexavalent Chromium [Cr (VI)]: A Health  
1210 Survey and Clinical Examination of Community Inhabitants (Kanpur, India). *PLOS*  
1211 *ONE*, 7(10), e47877. <https://doi.org/10.1371/journal.pone.0047877>

1212 Shi, X., & Dalal, N. S. (1990). On the hydroxyl radical formation in the reaction between  
1213 hydrogen peroxide and biologically generated chromium(V) species. *Archives of*

1214 *Biochemistry and Biophysics*, 277(2), 342–350. <https://doi.org/10.1016/0003->  
 1215 9861(90)90589-Q  
 1216 Siebach, K. L., Grotzinger, J. P., Kah, L. C., Stack, K. M., Malin, M., Léveillé, R., & Sumner,  
 1217 D. Y. (2014). Subaqueous shrinkage cracks in the Sheepbed mudstone: Implications for  
 1218 early fluid diagenesis, Gale crater, Mars. *Journal of Geophysical Research: Planets*,  
 1219 119(7), 1597–1613. <https://doi.org/10.1002/2014JE004623>  
 1220 Siebach, K. L., Baker, M. B., Grotzinger, J. P., McLennan, S. M., Gellert, R., Thompson, L.  
 1221 M., & Hurowitz, J. A. (2017). Sorting out compositional trends in sedimentary rocks of  
 1222 the Bradbury group (Aeolis Palus), Gale crater, Mars. *Journal of Geophysical Research:*  
 1223 *Planets*, 122(2), 295–328. <https://doi.org/10.1002/2016JE005195>  
 1224 Sillitoe, R. H. (2010). Porphyry Copper Systems. *Economic Geology*, 105(1), 3–41.  
 1225 <https://doi.org/10.2113/gsecongeo.105.1.3>  
 1226 Silverstone, S., Nelson, M., Alling, A., & Allen, J. (2003). Development and research program  
 1227 for a soil-based bioregenerative agriculture system to feed a four person crew at a Mars  
 1228 base. *Advances in Space Research*, 31(1), 69–75. <https://doi.org/10.1016/S0273->  
 1229 1177(02)00661-0  
 1230 Squyres, S. W., Aharonson, O., Clark, B. C., Cohen, B. A., Crumpler, L., de Souza, P. A., et al.  
 1231 (2007). Pyroclastic Activity at Home Plate in Gusev Crater, Mars. *Science*, 316(5825),  
 1232 738–742. <https://doi.org/10.1126/science.1139045>  
 1233 Squyres, S. W., Arvidson, R. E., Bell, J. F., Calef, F., Clark, B. C., Cohen, B. A., et al. (2012).  
 1234 Ancient Impact and Aqueous Processes at Endeavour Crater, Mars. *Science*, 336(6081),  
 1235 570–576. <https://doi.org/10.1126/science.1220476>  
 1236 Stack, K. M., Grotzinger, J. P., Kah, L. C., Schmidt, M. E., Mangold, N., Edgett, K. S., et al.  
 1237 (2014). Diagenetic origin of nodules in the Sheepbed member, Yellowknife Bay

1238 formation, Gale crater, Mars. *Journal of Geophysical Research: Planets*, 119(7), 1637–  
1239 1664. <https://doi.org/10.1002/2014JE004617>

1240 Stein, N., Grotzinger, J. P., Schieber, J., Mangold, N., Hallet, B., Newsom, H., et al. (2018).  
1241 Desiccation cracks provide evidence of lake drying on Mars, Sutton Island member,  
1242 Murray formation, Gale Crater. *Geology*, 46(6), 515–518.  
1243 <https://doi.org/10.1130/G40005.1>

1244 Stolper, E. M., Baker, M. B., Newcombe, M. E., Schmidt, M. E., Treiman, A. H., Cousin, A.,  
1245 et al. (2013). The Petrochemistry of Jake\_M: A Martian Mugearite. *Science*, 341(6153),  
1246 1239463–1239463. <https://doi.org/10.1126/science.1239463>

1247 Sun, V. Z., Stack, K. M., Kah, L. C., Thompson, L., Fischer, W., Williams, A. J., et al. (2019).  
1248 Late-stage diagenetic concretions in the Murray formation, Gale crater, Mars. *Icarus*,  
1249 321, 866–890. <https://doi.org/10.1016/j.icarus.2018.12.030>

1250 Taylor, S. R., & McLennan, S. (2009). *Planetary Crusts: Their Composition, Origin and*  
1251 *Evolution*. Cambridge: Cambridge University Press.  
1252 <https://doi.org/10.1017/CBO9780511575358>

1253 Thompson, L., Berger, J. A., Boyd, N., Gellert, R., M, A., McCraig, et al. (2020). The Murray  
1254 formation , Gale crater , Mars : APXS compositional analysis reveals element gains and  
1255 losses and multiple diagenetic events. Presented at the LPSC, The Woodlands, TX,  
1256 United States. Retrieved from /paper/The-Murray-formation-%2C-Gale-crater-%2C-  
1257 Mars-%3A-APXS-Thompson-Berger/04cb3c4b1e2b4cc0fbc524977e594fcd394efa5e

1258 Thomson, B. J., Bridges, N. T., Milliken, R., Baldrige, A., Hook, S. J., Crowley, J. K., et al.  
1259 (2011). Constraints on the origin and evolution of the layered mound in Gale Crater,  
1260 Mars using Mars Reconnaissance Orbiter data. *Icarus*, 214(2), 413–432.  
1261 <https://doi.org/10.1016/j.icarus.2011.05.002>

1262 Thorpe, M., Bristow, T., Rampe, E. B., Blake, D. F., Vaniman, D., Yen, A., et al. (2020).  
1263 Mineralogy of the Glen Torridon Region as detailed by the Mars Science Laboratory  
1264 CheMin Instrument. Presented at the AGU Fall Meeting 2020, AGU. Retrieved from  
1265 <https://agu.confex.com/agu/fm20/meetingapp.cgi/Paper/700645>

1266 Treiman, A. H., Bish, D. L., Vaniman, D. T., Chipera, S. J., Blake, D. F., Ming, D. W., et al.  
1267 (2016). Mineralogy, provenance, and diagenesis of a potassic basaltic sandstone on  
1268 Mars: CheMin X-ray diffraction of the Windjana sample (Kimberley area, Gale Crater).  
1269 *Journal of Geophysical Research: Planets*, 121(1), 75–106.  
1270 <https://doi.org/10.1002/2015JE004932>

1271 Tuff, J., Wade, J., & Wood, B. J. (2013). Volcanism on Mars controlled by early oxidation of  
1272 the upper mantle. *Nature*, 498(7454), 342–345. <https://doi.org/10.1038/nature12225>

1273 Udry, A., Howarth, G. H., Herd, C. D. K., Day, J. M. D., Lapen, T. J., & Filiberto, J. (2020).  
1274 What martian meteorites reveal about the interior and surface of Mars. *Journal of*  
1275 *Geophysical Research: Planets*, n/a(n/a), e2020JE006523.  
1276 <https://doi.org/10.1029/2020JE006523>

1277 Udry, Arya, Gazel, E., & McSween, H. Y. (2018). Formation of Evolved Rocks at Gale Crater  
1278 by Crystal Fractionation and Implications for Mars Crustal Composition. *Journal of*  
1279 *Geophysical Research: Planets*, 123(6), 1525–1540.  
1280 <https://doi.org/10.1029/2018JE005602>

1281 VanBommel, S. J., Gellert, R., Berger, J. A., Thompson, L. M., Edgett, K. S., McBride, M. J.,  
1282 et al. (2017). Modeling and mitigation of sample relief effects applied to chemistry  
1283 measurements by the Mars Science Laboratory Alpha Particle X-ray Spectrometer. *X-*  
1284 *Ray Spectrometry*, 46(4), 229–236. <https://doi.org/10.1002/xrs.2755>

1285 Vaniman, D. T., Bish, D. L., Ming, D. W., Bristow, T. F., Morris, R. V., Blake, D. F., et al.  
 1286 (2014). Mineralogy of a Mudstone at Yellowknife Bay, Gale Crater, Mars. *Science*,  
 1287 343(6169), 1243480–1243480. <https://doi.org/10.1126/science.1243480>  
 1288 Varma, S. J., Muchowska, K. B., Chatelain, P., & Moran, J. (2018). Native iron reduces CO<sub>2</sub>  
 1289 to intermediates and end-products of the acetyl-CoA pathway. *Nature Ecology &*  
 1290 *Evolution*, 2(6), 1019–1024. <https://doi.org/10.1038/s41559-018-0542-2>  
 1291 Wamelink, G. W. W., Frissel, J. Y., Krijnen, W. H. J., & Verwoert, M. R. (2019). Crop growth  
 1292 and viability of seeds on Mars and Moon soil simulants. *Open Agriculture*, 4(1), 509–  
 1293 516. <https://doi.org/10.1515/opag-2019-0051>  
 1294 Wamelink, G. W., Wieger, Frissel, J. Y., Krijnen, W. H. J., Verwoert, M. R., & Goedhart, P. W.  
 1295 (2014). Can Plants Grow on Mars and the Moon: A Growth Experiment on Mars and  
 1296 Moon Soil Simulants. *PLOS ONE*, 9(8), e103138.  
 1297 <https://doi.org/10.1371/journal.pone.0103138>  
 1298 WHO. (2003). *Chromium in drinking-water*. World Health Organization. Retrieved from  
 1299 WHO/SDE/WSH/03.04/04  
 1300 Wiens, R. C., Meslin, P.-Y., Wellington, D. F., Johnson, J. R., Fraeman, A., Gasnault, O., et al.  
 1301 (2017). Composition and Morphology of Iron Meteorites Found in Gale Crater, Mars.  
 1302 In *80th Annual Meeting of the Meteoritical Society* (Vol. 1987, p. 6168). Retrieved from  
 1303 <http://adsabs.harvard.edu/abs/2017LPICo1987.6168W>  
 1304 Wiens, Roger C., Maurice, S., Barraclough, B., Saccoccio, M., Barkley, W. C., Bell, J. F., et al.  
 1305 (2012). The ChemCam Instrument Suite on the Mars Science Laboratory (MSL) Rover:  
 1306 Body Unit and Combined System Tests. *Space Science Reviews*, 170(1–4), 167–227.  
 1307 <https://doi.org/10.1007/s11214-012-9902-4>  
 1308 Wiens, Roger C., Maurice, S., Robinson, S. H., Nelson, A. E., Cais, P., Bernardi, P., et al.  
 1309 (2020). The SuperCam Instrument Suite on the NASA Mars 2020 Rover: Body Unit

and Combined System Tests. *Space Science Reviews*, 217(1), 4.  
<https://doi.org/10.1007/s11214-020-00777-5>

Winterhalter, D., Levine, J. S., & Kerschmann, R. (2018). *The Dust in the Atmosphere of Mars and Its Impact on the Human Exploration of Mars: A NESC Workshop*.

Yang, S., Humayun, M., Richter, K., Jefferson, G., Fields, D., & Irving, A. J. (2015). Siderophile and chalcophile element abundances in shergottites: Implications for Martian core formation. *Meteoritics & Planetary Science*, 50(4), 691–714.  
<https://doi.org/10.1111/maps.12384>

Yen, A. S., Mittlefehldt, D. W., McLennan, S. M., Gellert, R., Bell, J. F., McSween, H. Y., et al. (2006). Nickel on Mars: Constraints on meteoritic material at the surface: NICKEL ON MARS. *Journal of Geophysical Research: Planets*, 111(E12), n/a-n/a.  
<https://doi.org/10.1029/2006JE002797>

Zubrin, R. (2011). *Case for Mars*. Simon and Schuster.

## Figures

**Figure 1.** Elevation map of the surface of Mars obtained by the Mars Orbiter Laser Altimeter (MOLA). Locations of interest are indicated with an empty circle.

**Figure 2.** (a) Context Camera (CTX) mosaic of Gale crater. (b) Stratigraphic column modified from the Sed/Strat MSL group. Locations of interests are indicated in dark blue.

K and YB formation in the Bradbury group correspond to the Kimberley and Yellowknife Bay formations, respectively.

**Figure 3.** Images of (a) the Windjana drilling site with Blina, Stephen, and Neil ChemCam targets indicated, (b) Stephen, (c) Neil, and (d) Mondooma fracture fills containing elevated MnO, Ni, Zn, and Cu concentrations. The red annotations on images (b-d) show the locations of the LIBS analyses.

**Figure 4.** MAHLI mosaic of a vein in the Garden City vein complex. The white materials correspond to Ca-sulfate and the dark materials contain elevated Ge and Mn concentrations.

**Figure 5.** (a) Image of an iron-rich meteorite called Lebanon (sol 640). This image is a combination of the colored MastCam images and high resolution Remote Micro Imager (RMI) images, which are outlined with white lines. (b) RMI image of a Fe-meteorite (sol 1376). Red numbers correspond to LIBS analyses. The arrow indicates the location of the corresponding



LIBS average spectrum that is centered around (c) the Fe lines and (d) the Ni lines. The LIBS spectrum corresponds to the average of 24 LIBS shots (6-30 to avoid dust contamination in the first 5 shots; Lasue et al., 2013) performed in point 2, which was then normalized to the entire spectrum.

**Figure 6.** Sketch illustrating the functioning of the photosystem II. ADP is for adenosine diphosphate, and ATP for adenosine triphosphate. Stroma is the fluid within plant and some algae cells (chloroplasts) that produces energy. Lumen corresponds to an aqueous phase surrounded by a membrane. The Calvin cycle is a serie of reactions that happens within chloroplasts during photosynthesis.

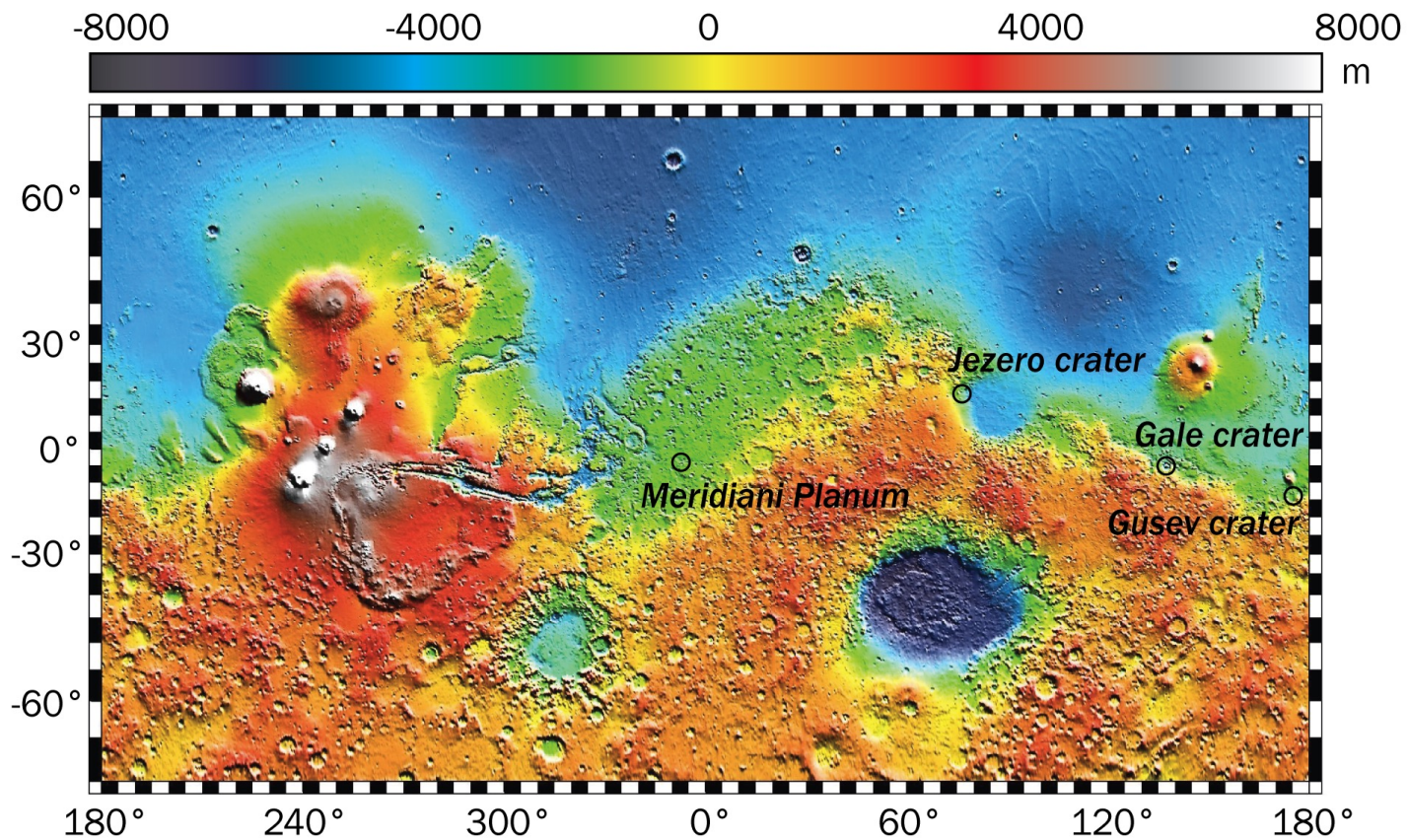


Fig. 1. Elevation map of the surface of Mars obtained by the Mars Orbiter Laser Altimeter (MOLA). Locations of interest are indicated with an empty circle.

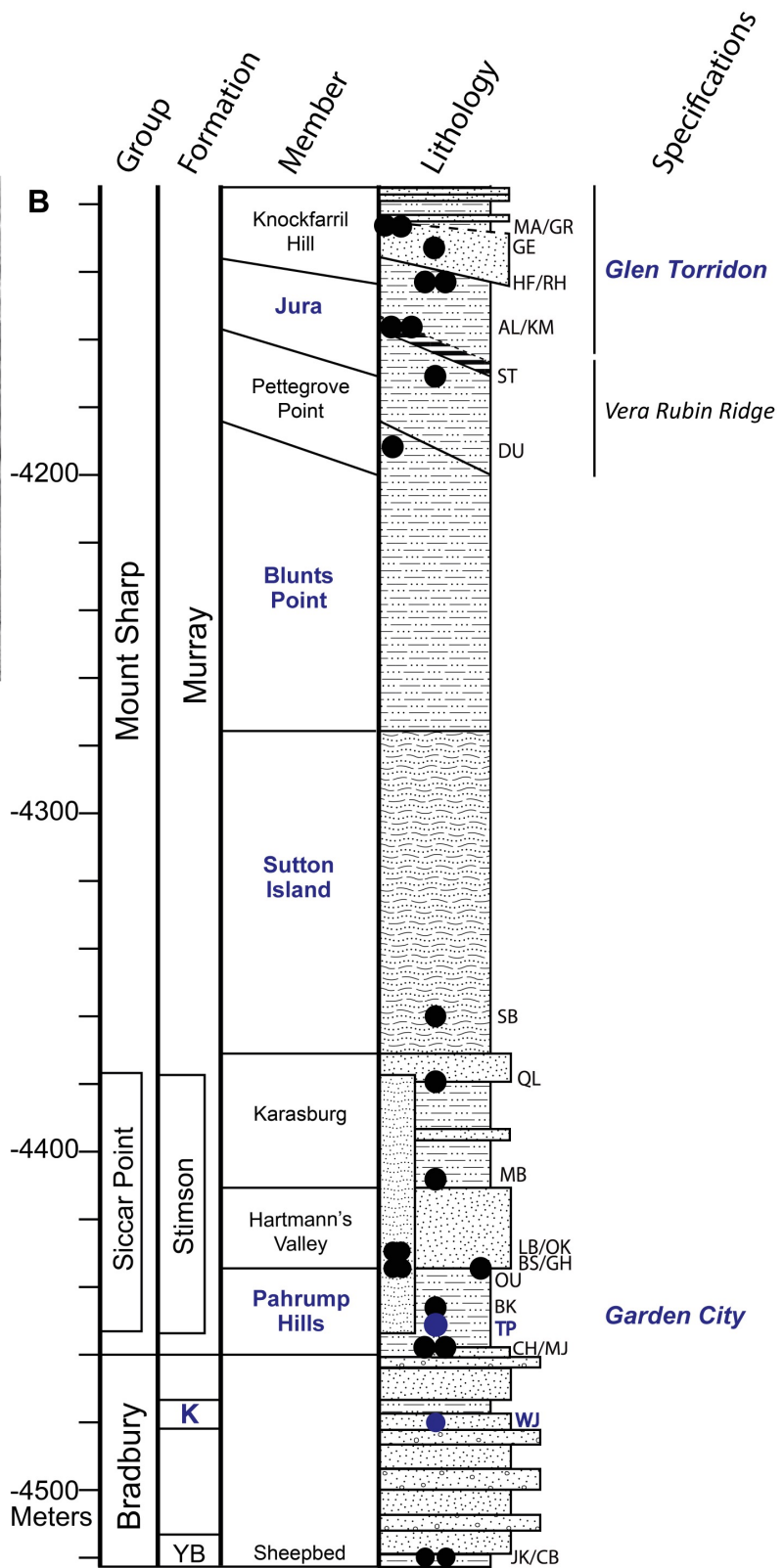
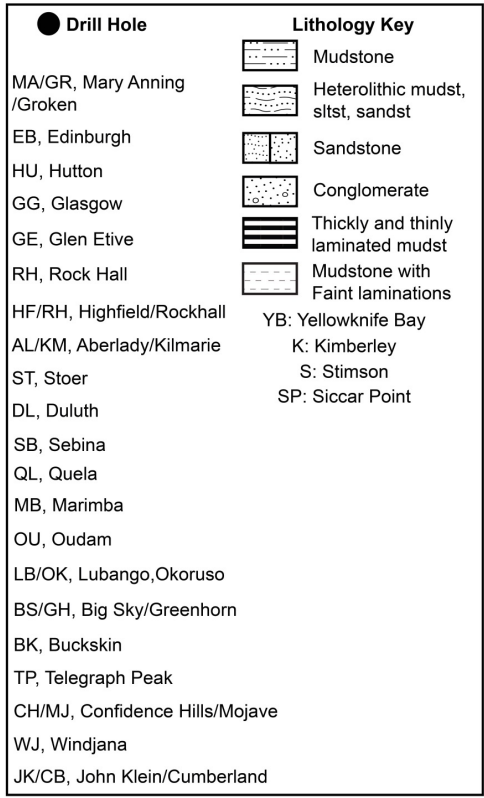
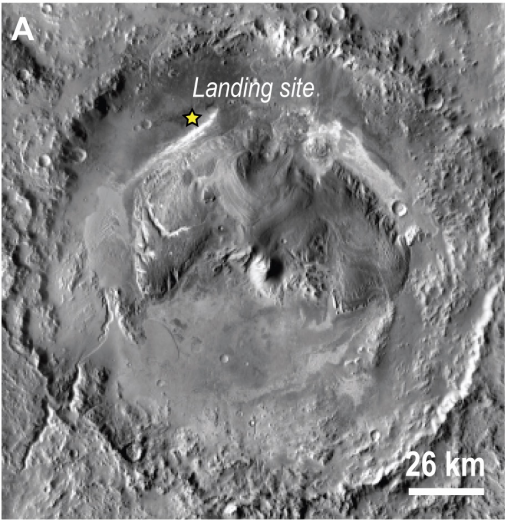


Fig. 2. (a) Context Camera (CTX) mosaic of Gale crater. (b) Stratigraphic column modified from the Sed/Strat MSL group. Locations of interests are indicated in dark blue. K and YB formation in the Bradbury group correspond to the Kimberley and Yellowknife Bay formations, respectively.



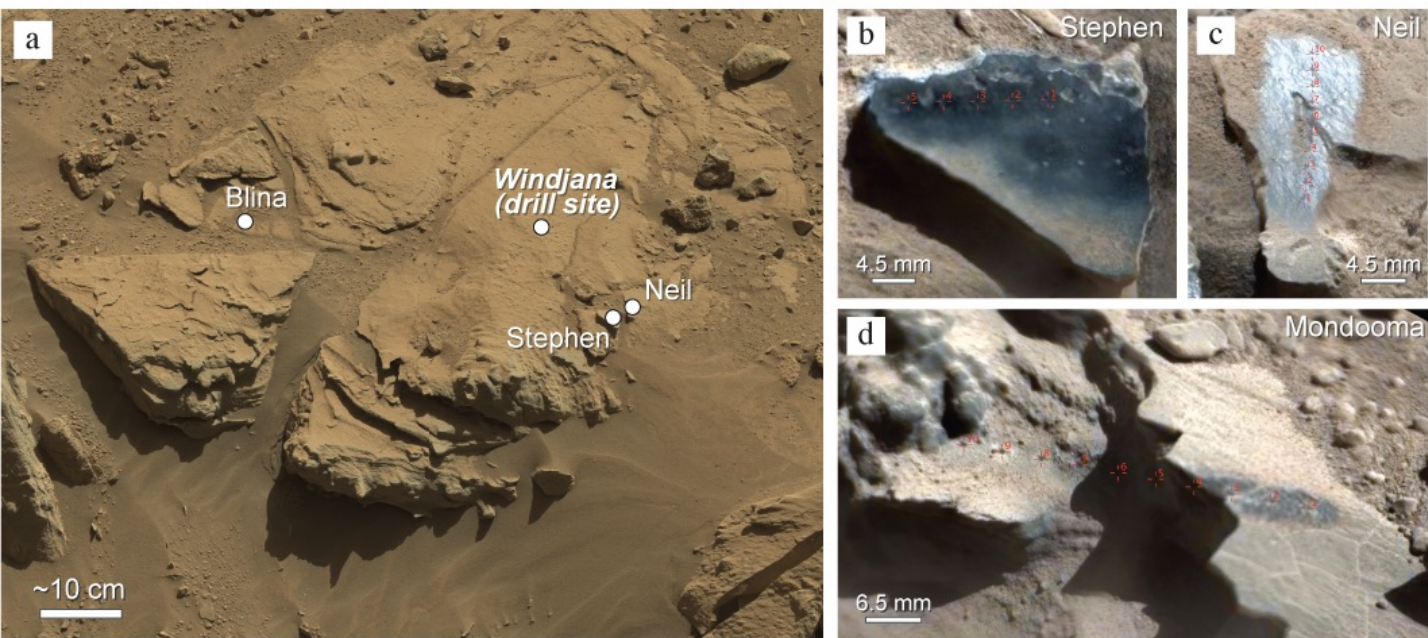


Fig. 3. Images of (a) the Windjana drilling site with Blina, Stephen, and Neil ChemCam targets indicated, (b) Stephen, (c) Neil, and (d) Mondooma fracture fills containing elevated MnO, Ni, Zn, and Cu concentrations. The red annotations on images (b-d) show the locations of the LIBS analyses.

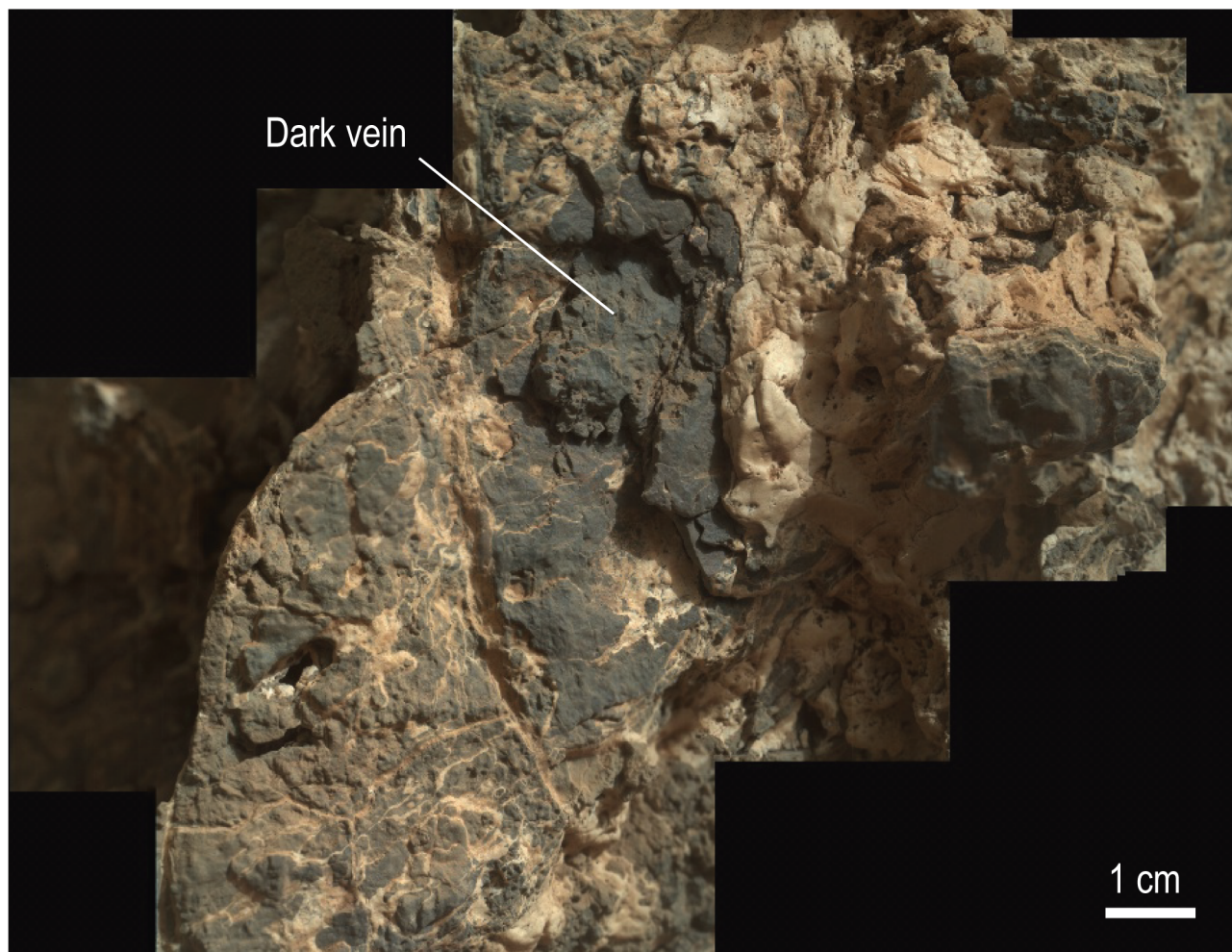


Fig. 4. MAHLI mosaic of a vein in the Garden City vein complex. The white materials correspond to Ca-sulfate and the dark materials contain elevated Ge and Mn concentrations.



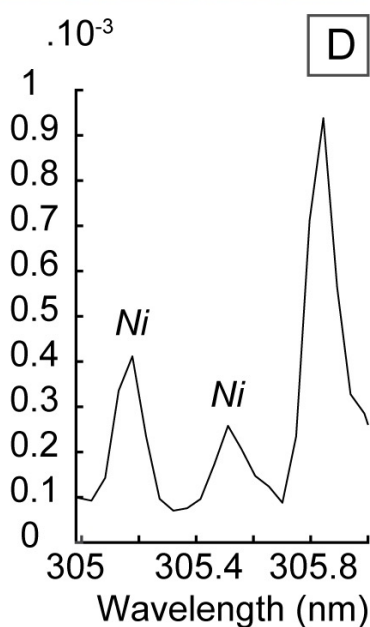
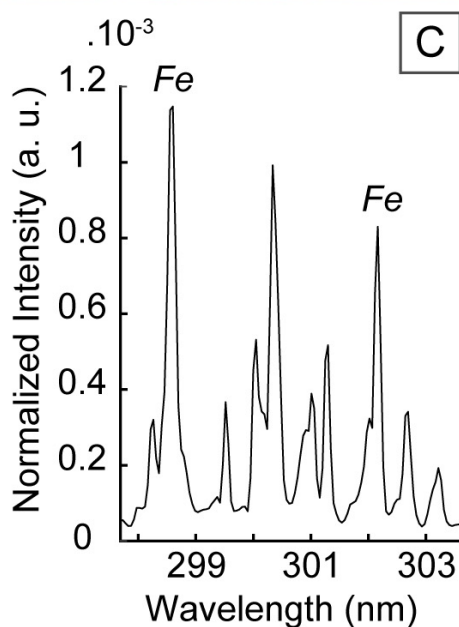
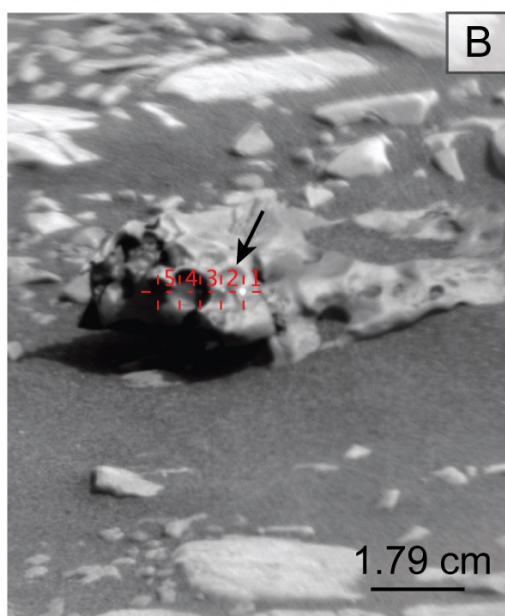


Fig. 5. (a) Image of an iron-rich meteorite called Lebanon (sol 640). This image is a combination of the colored MastCam images and high resolution Remote Micro Imager (RMI) images, which are outlined with white lines. (b) RMI image of a Fe-meteorite (sol 1376). Red numbers correspond to LIBS analyses. The arrow indicates the location of the corresponding LIBS average spectrum that is centered around (c) the Fe lines and (d) the Ni lines. The LIBS spectrum corresponds to the average of 24 LIBS shots (6-30 to avoid dust contamination in the first 5 shots; Lasue et al., 2013) performed in point 2, which was then normalized to the entire spectrum.

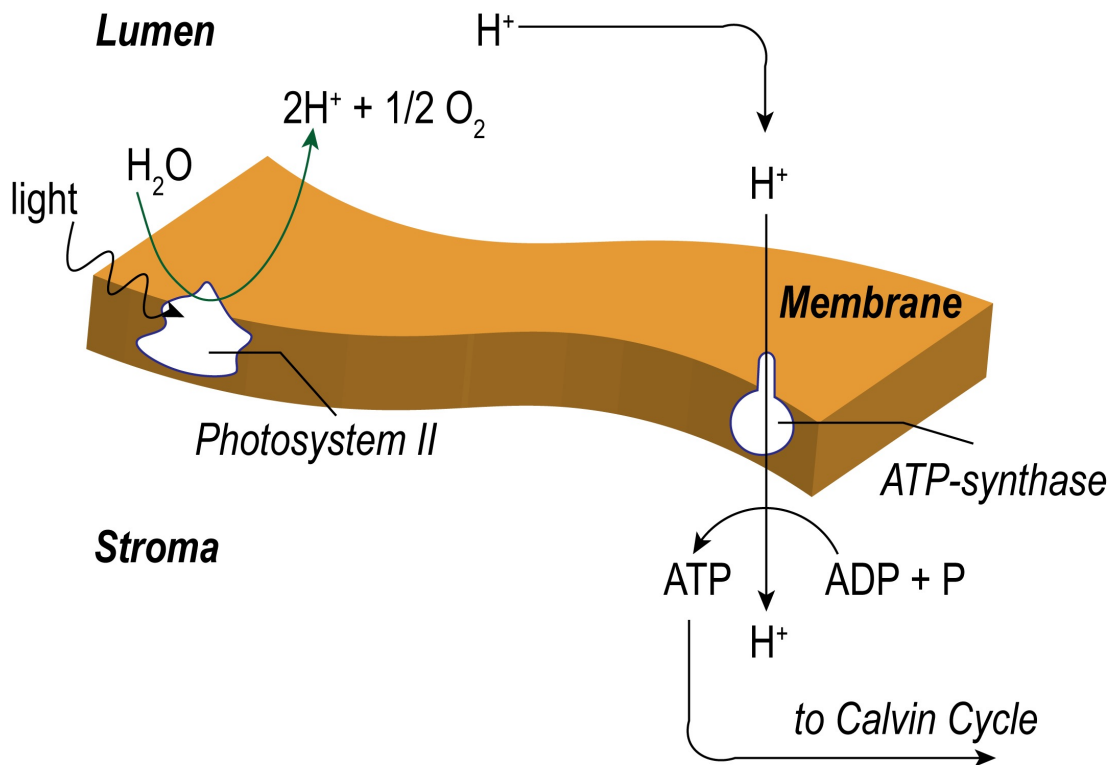


Fig. 6. Sketch illustrating the functioning of the photosystem II. ADP is for adenosine diphosphate, and ATP for adenosine triphosphate. Stroma is the fluid within plant and some algae cells (chloroplasts) that produces energy. Lumen corresponds to an aqueous phase surrounded by a membrane. The Calvin cycle is a series of reactions that happens within chloroplasts during photosynthesis.